NTNU – Trondheim
Norwegian University of
Science and Technology

Experimental Studies of Instabilities Near the Sol-Gel Transition

Kristian Hox

Master of Science in Physics and Mathematics
Submission date: June 2012
Supervisor: Jon Otto Fossum, IFY

Norwegian University of Science and Technology
Department of Physics

Abstract

This master thesis presents a new experimental way to dynamically determine rheological properties of a complex fluid. The fluid investigated is a suspension of the synthetic clay mineral laponite of 3 wt%. This is mixed together with distilled water or a NaCl solution with concentrations bellow 10^{-2} M. Laponite gels are thixotropic and shear thinning with a yield stress. In the experiments done during this thesis the transition between liquid and solid behavior is investigated using a Hele-Shaw cell and a rheometer. Three different phases is observed with respect to waiting time and NaCl concentration. These are recognized as a liquid phase for small concentration of NaCl and short waiting times and a solid phase for high concentration of NaCl and long waiting time. In the intermediate range a viscoelastic phase is observed.

Some experiments were done with the sample placed between crossed polarizers, and birefringence was observed in all three phases. In the solid phase it is observed only a small area around the fracture tip. In the liquid phase this is observed in front of the finger, but this is not a stable phase. In the viscoelastic regime a stable nematic phase occur along the stress field around the interface of the bubble. This nematic phase will align normal to the glass surface. Fracture like patterns in the nematic phase are observed. This is an elastic behavior with the clay platelets aligning normal to the stress field to prepare for fractures to propagate there.

Different NaCl concentrations will give different arrested states, respectively a repulsive glass and a attractive gel. It is expected that glass and gels behave differently in this experiment, but this was not confirmed. A gel phase have been observed in concentrations of NaCl above $5 \cdot 10^{-3}$ for waiting times up to 605 hours. For smaller concentrations a even longer waiting time is expected and experiments on this needs to be performed in future studies.

In addition this experiment could investigate and give insight of flow in complex fluid. To investigate this further, tracer particles have been used in a few experiments. The results are promising for further studies.

In this thesis work, a large range in waiting times and concentrations of NaCl have been investigated. In future studies it should be carried out experiments in a smaller range of these parameters along with other parameters. Also a more quantitative analysis should be carried out. Especially the transitions between fluid/viscoelastic and viscoelastic/solid is interesting to investigate further.

Sammendrag

Denne masteroppgaven presenterer en ny eksperimentell måte å dynamisk bestemme de reologiske egenskapene til en kompleks væske. Væsken undersøkt er en løsning med 3 wt% av den syntetiske leiren laponite sammen med destillert vann eller en NaCl-løsning med konsentrasjoner under 10^{-2} M. Laponite er en tiksotrop og skjær tynnende leire med flytespenning . I forsøkene gjort i løpet av denne oppgaven er overgangen mellom flytende og fast stoff undersøkt i en Hele-Shaw celle og i et reometer. Tre forskjellige faser observeres med hensyn til ventetid og konsentrasjon av NaCl, en væskefase for små konsentrasjoner av NaCl og kort ventetid og en fast fase for høye konsentrasjoner av NaCl og lang ventetid. Mellom disse er en viskoelastisk fase.

Eksperimenter gjort med kryssede polarisatorer viser dobbelt brytning i alle tre fasene. I den faste fasen er det bare et lite område rundt sprekkens tupp som viser dette. I væskefasen er dette observert foran fingeren, men dette er ikke en stabil fase. I det viskoelastiske regimet er det en stabil nematisk fase som dannes langs spenningsfeltet rundt overflaten til boblen. Leireplatene vil innrette seg normalt på glassflaten. Mønstre som ligner på sprekker i den nematiske fasen er observert. Dette er en elastisk oppførsel av leire plater som innstiller seg normalt på spenningsfeltet for å forberede at sprekker kan utbre seg der.

Ulike NaCl konsentrasjoner vil gi ulike faste tilstander, henholdsvis et frastøtende glass og en attraktiv gel. Det forventes at glass og geler oppfører seg annerledes i dette eksperimentet, men dette er ikke bekreftet. En gel-fase har vært observert i konsentrasjoner av NaCl over $5 \cdot 10^{-3}$ for ventetider på opptil 605 timer. For mindre konsentrasjoner er det forventet en enda lengre ventetid og eksperimenter på dette burde utføres i videre observasjoner.

I tillegg kan dette eksperimentet undersøke og gi innsikt i strømning i kompleks væske. For å undersøke dette nærmere er sporingpartikler blitt brukt i noen få eksperimenter. Disse eksperimentene ser lovende ut for videre studier.

I denne masteroppgaven er et stort spekter i ventetider og konsentrasjoner av NaCl undersøkt. I videre studier bør et mindre spekter av disse parametrene undersøkes og analyseres kvantitativt. Spesielt overgangene mellom væske/viskoelastisk og viskoelastisk/fast vil være interessante å undersøke nærmere.

Contents

List of Figures

Preface

The work presented in this Master thesis is performed during the tenth semester of my Master's degree in Applied Physics and Mathematics at the Norwegian University of Science and Technology (NTNU) and has been carried out at the Complex Systems and Soft Materials group at the Department of Physics.

The study have been done in cooperation with PhD Baudouin Saintyves and his supervisor Elisabeth Bouchaud at CEA Saclay. I am grateful for all professional discussions and help I have got from them.

I also thank engineer Daniel Skåre in the Optics group at NTNU for measuring the Mueller matrix of my quarter-wave sheet.

I would like to thank my supervisor Professor Jon Otto Fossum for everything he has taught me about clay-systems and all the guidance through this work. I will also thank post doc Zbigniew Rozynec for help with the rheometer and the group's technician Ole Tore Buseth for helping me with the setup.

I am really grateful to my girlfriend Anne Mette that helped me proofread my thesis and motivating me through this work.

Trondheim, 15. June 2012 Kristian Hox

Chapter 1

Introduction

This master thesis presents the result of studies done on instabilities in non-newtonian fluids. It is a continuation of the work done by Beate Cappelen during her master thesis [1] and my ninth semester project in the fall of 2011.

The system studied is a clay suspension of the synthetic clay mineral laponite. This is a clay with a exiting phase diagram and several different solid states could be reached with different clay and salt concentration and laponite is one of the most studied clay systems. It is homogenous and the behavior of the clay is strongly time-dependent. For low concentrations of laponite in distilled water the process is slow and on the year scale[2, 3]. During time the viscous and elastic properties will change. The study about elasticity and viscosity is called rheology and more about rheology could be found in section 2.1.

Many thing is known about laponite but many things still needs an explanation. One of these things is the viscoelastic behavior when stress is applied and this would be investigated in this thesis were we have linked the patterns formed to elastic and viscous properties. More about clay is found in section 2.7. The transition between a solvent and a solid state is called the sol-gel transition and could be read more about in section 2.2.

The motivation for the study done in this thesis is to get a better understanding of flow and pattern formation of fingers and fractures in a two-phase system. Two-phase systems are a very common process in various industries. The analogy between the Hele-Shaw cell and porous media is known so much of this could be linked to the petroleum industry and flow in oil reservoirs. For example a common way to recover more oil is to drill several wells and pump water into the reservoir. At the interface between water and oil it is typical to see water brake through to the pumping well as fingers of water penetrating the oil [4]. More about fracturing, fingering and the Hele-Shaw cell in section 2.3, 2.4 and 2.5.

Chapter 3 will give a description of the experimental work including preparation of clay. The protocol of preparing clay is changed from my project report. To make a reproducible initial state the clay is dried and prepared under a N_2 environment in a glove bag to determine the concentration of laponite accurate. The solvent is also filtered to dissolve the clay powder completely. In addition to investigate the pattern experiments are done with both crossed linear and crossed circular polarizers and with tracer particles. Some experiments is also performed in a rheometer. In chapter 4 the results obtained is presented and discussed. The conclusion is found together with a proposal of future studies in chapter 5. In appendix A a summary of the notation used in this report is found.

Parts of this work was presented on a international workshop on 'Soft matter physics and complex flows' in Lofoten 22.-25. May 2012. The poster is found in appendix E.

Chapter 2

Theory

2.1 Rheology

The term rheology was defined in 1929 as *the study of the deformation and flow of matter* [5]. Rheology is the description of the behavior of matter when forces or stress is applied [6]. Matter could be either solid, liquid or gas. In one end of the spectrum there is ideal solids and on the other ideal fluids. Fluid could be both liquid and gas.

Ideal solids deform elastically, this means that it will recover when stress is removed and is described in the following equation:

$$\boldsymbol{\sigma} = G\boldsymbol{\gamma} \tag{2.1}$$

Here $\boldsymbol{\sigma}$ is the shear stress, $\boldsymbol{\gamma}$ is the strain and G is the shear modulus. Ideal fluids on the other hand deforms irreversible and do not recover when stress is removed. Ideal fluids are also called Newtonian fluids and are described by:

$$\boldsymbol{\sigma} = \eta\dot{\boldsymbol{\gamma}} \tag{2.2}$$

Here $\boldsymbol{\sigma}$ is still the shear stress, $\dot{\boldsymbol{\gamma}}$ is the shear rate and η is the viscosity constant. One can also argue that a solid can be treated as a fluid with $\eta \to \infty$ [6]. In three dimension Newtonian flow is described by Navier-Stokes equations [7].

Generally $\boldsymbol{\sigma}$ is three-dimensional and divided into nine components as shown in Figure 2.1. Here the first index of σ_{nm} refers to the orientation of the surface and the second refers to the direction of the stress. Components with both index equal (σ_{xx}, σ_{yy} and σ_{zz}) are called normal stresses and the other are called shear stresses [5]. Symmetry implies that there are only three independent components of shear stress and these are σ_{xy}, σ_{xz} and σ_{yz}. It is usual to use normal stress differences rather than normal stress [6]. These are defined as:

$$N1 = \sigma_{xx} - \sigma_{yy} \tag{2.3}$$

$$N2 = \sigma_{yy} - \sigma_{zz} \tag{2.4}$$

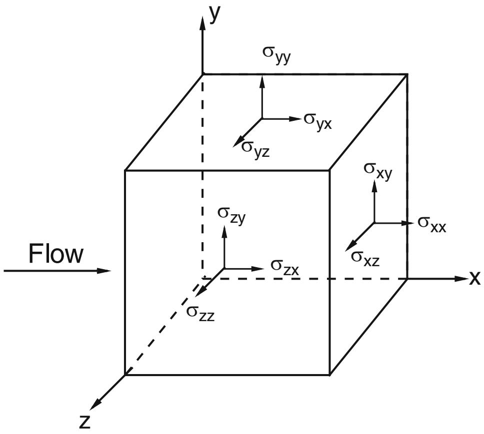

Figure 2.1: Stress components in three-dimensional flow. Figure adapted from [6].

2.1.1 Non-Newtonian fluids

Most liquids are not ideal but someplace between a fluid and a solid. They will both flow and deform elastically in some way. That is why we call them viscoelastic, non-Newtonian, non-linear or just complex fluids [6, 7]. To describe how elastic or viscous a non-Newtonian fluid is, the dimensionless Deborah number D_e is used. This is defined as:

$$D_e = \text{time of relaxation/time of observation} \tag{2.5}$$

A material can behave solid-like or fluid-like based on how large or small the Deborah number is. For an ideal solid the time of relaxation and D_e is infinite and for a ideal fluid the time of relaxation and D_e is zero. For all practical reasons the material can be considered as solid when the time of relaxation is larger than the time of observation ($D_e < 1$) [5, 8].

The relationship between shear stress and shear rate do not need to be linear and the viscosity, $\eta = \sigma/\dot{\gamma}$, is generally dependent on six independent parameters; S, T, p, $\dot{\boldsymbol{\gamma}}$, t, and $\boldsymbol{E}$. Here S is the physical-chemical nature of the substance, T is temperature, p is the pressure, $\dot{\boldsymbol{\gamma}}$ is the shear rate, t is the time and $\boldsymbol{E}$ is the electric field. Often several of these parameters could be neglected. It is usually to distinguish between time-dependent and time-independent behavior [7].

Time-independent fluid behavior

Effects that is not dependent on time could be thought of as processes with no memory and there are three possibilities regarding shear rate. These are shear-thinning/pseudoplastic behavior, shear-thickening/dilatant behavior or viscoplastic behavior with or without shear-thinning. An overview of this is shown in Figure 2.2 together with the line for a Newtonian fluid [6].

There are several different models that characterize this. The simplest one is the power law model or Ostwald de Waele equation:

$$\eta = m\dot{\gamma}^{n-1} \tag{2.6}$$

This will give a straight line over an interval. For small intervals in shear rate this could be a good model, but for larger range of shear rate this could be bad. Other models that could be mentioned are the Ellis fluid model, the cross model and the Sisko model. A comparison of three of these models are shown in Figure 2.3 [5].

For the viscoplastic behavior there is a threshold stress, σ_0, that must be exceeded for the fluid to flow. When this is exceeded there could be behavior similar to newtonian fluid flow(Bingham plastic) or shear-thinning behavior. Two models used in this case is the Herschel-Bulkley fluid model and the

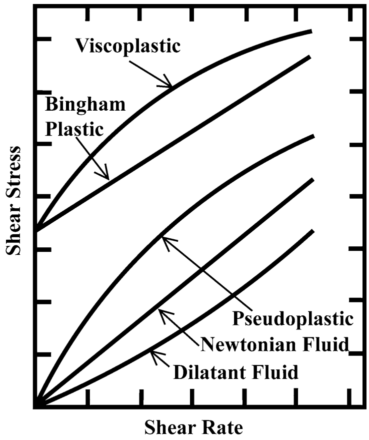

Figure 2.2: Qualitatively the flow curves for a newtonian fluid and the different categories of non-newtonian time-independent fluids. Figure adapted from [6].

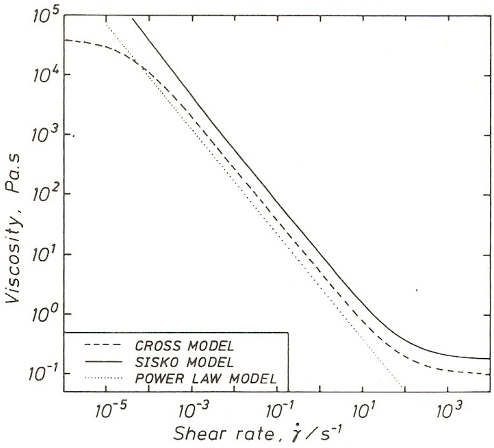

Figure 2.3: Comparison of shear rate graph for three different models. The Cross model, the Sisko model and the power law model. For clarity the graph has been shifted. Figure adapted from [5].

Casson model. The Herschel-Bulkley model is described with the following equation:

$$\eta = \frac{\sigma_0}{\dot{\gamma}} + K\dot{\gamma}^{n-1} \tag{2.7}$$

Where K represents the consistency factor and n represent how shear thinning the system is. If $n = 1$ the equation represent the Bingham plastic [5, 6, 9].

Time-dependent fluid behavior

In many cases the shear stress also is time-dependent. It is normal to divide this in to two types, thixotropic behavior and rheopectic behavior. There is only found a few fluids with rheopectic behavior but thixotropy is quite normal. Rheopectic behavior is also called anti-thixotropy. The difference between them is shown in Figure 2.4. Here the samples are applied steadily increasing shear and then decreasing at the same rate. If the sample shows no time-dependency, the lines would lay on top of each other. In the figure this is not the case.

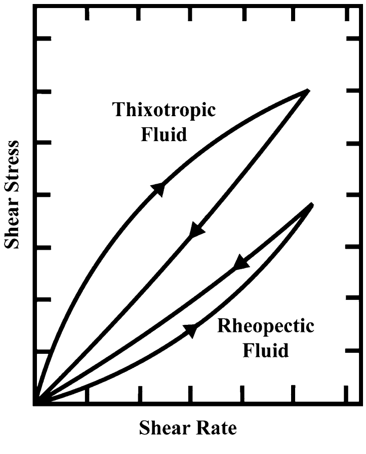

Figure 2.4: Flow curve for thixotropic and rheopectic behavior. Figure adapted from [6].

Thixotropy could be explained with that due to shear, internal structures are broke down so the stress will be less as time goes by when shearing at the same rate. This is in some cases reversible, so over a long period of rest structures are rebuild and fluid could regain initial values of rheology parameters [6].

2.1.2 Linear viscoelasticity

Viscoelasticity means a material that shows both viscous and elastic behavior. In other word a general viscoelastic model contains both Newtonian, Hookean and materials in between. In the linear viscoelasticity theory the differential equation with respect to time is linearly dependent with constant coefficients. This do that the linear theory only is valid over a small range of other parameters as temperature, pressure and electrical fields. The general equation is shown in equation (2.8). Here σ and γ can be replaced with general tensors to give flow in all directions [5].

$$\begin{aligned}&\left(1+\alpha_1\frac{\partial}{\partial t}+\alpha_2\frac{\partial^2}{\partial t^2}+\cdots+\alpha_n\frac{\partial^n}{\partial t^n}\right)\sigma\\ &=\left(1+\beta_1\frac{\partial}{\partial t}+\beta_2\frac{\partial^2}{\partial t^2}+\cdots+\beta_m\frac{\partial^m}{\partial t^m}\right)\gamma\end{aligned} \tag{2.8}$$

Here some important cases are described. If β_0 is the only non-zero coefficient we get:

$$\sigma=\beta_0\gamma \tag{2.9}$$

That is the same as the equation for an ideal solid with $\beta_0 = G$, see equation (2.1). Next if β_1 is the only non-zero coefficient we get:

$$\sigma=\beta_1\frac{\partial\gamma}{\partial t}=\beta_1\dot{\gamma} \tag{2.10}$$

That is the same as for an ideal fluid with $\beta_1 = \eta$, see equation (2.2). The simplest model of linear viscoelasticity is when combining these two, e.g. $\beta_0 = G$, $\beta_1 = \eta$ and all other coefficient are zero. This is known as the Kelvin model or Voigt model [5, 6]:

$$\sigma=G\gamma+\eta\dot{\gamma} \tag{2.11}$$

It could be shown that the following applies to the Kelvin model:

$$\gamma=\frac{\sigma}{G}\left(1-\mathrm{e}^{-t/\tau_K}\right) \tag{2.12}$$

Where $\tau_K = \eta/G$ is called the retardation time.

Another simple model is the Maxwell model. Here $\alpha_1 = \tau_M$ is called the relaxation time, $\beta_1 = \eta$ and all other coefficient are zero:

$$\sigma + \tau_M \dot{\sigma} = \eta\gamma \tag{2.13}$$

The following is true for shear stress:

$$\sigma = \eta\dot{\gamma}\mathrm{e}^{-t/\tau_M} \tag{2.14}$$

It is normal to picture Hookean elasticity with a spring and Newtonian flow with a dashpot. This is shown in Figure 2.5. The Kelvin model and Maxwell model could then be pictured by respectively a parallel and a serial of these two. This is shown in Figure 2.6.

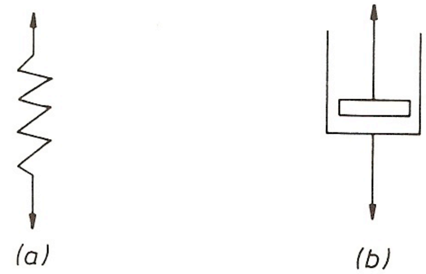

Figure 2.5: Schematic representation of (a) an ideal solid represented by an Hookean spring and (b) an ideal fluid represented by the Newtonian dashpot. Figure adapted from [5].

It is possible to expand this to models containing three or more parameters, but this could also easy be expanded to a 'generalized Kelvin' and 'generalized Maxwell' model. This could be done by rewriting equation (2.11) and (2.13) and sum over n of this elements using the superposition principle. This gives the following equation for the 'generalized Kelvin' model:

$$\gamma(t) = \sum_{i=1}^{n} \frac{1}{\eta_i} \int_{-\infty}^{t} \mathrm{e}^{-(t-t')/\tau_i} \sigma(t')\mathrm{d}t' \tag{2.15}$$

And for the 'generalized Maxwell' model:

$$\sigma(t) = \sum_{i=1}^{n} \frac{\eta_i}{\tau_i} \int_{-\infty}^{t} \mathrm{e}^{-(t-t')/\tau_i} \dot{\gamma}(t')\mathrm{d}t' \tag{2.16}$$

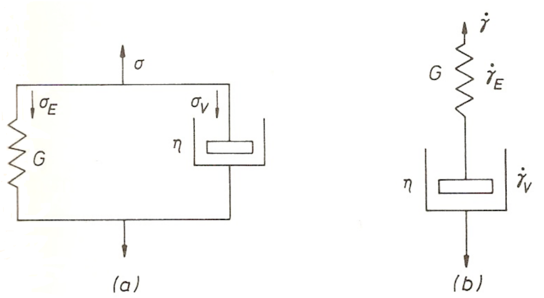

Figure 2.6: Schematic representation of (a) the Kelvin model with an Hookean spring and an Newtonian dashpot in parallel and (b) the Maxwell model with an Hookean spring and an Newtonian dashpot in serial. Figure adapted from [5].

To determine the parameters in this model, oscillatory shear measurement in a rheometer is often used [5, 6].

Oscillatory shear

In a oscillatory shear test a harmonic strain is applied to the sample where ω is the angular frequency that is applied:

$$\gamma(t) = \gamma_0 \mathrm{e}^{i\omega t} \tag{2.17}$$

And the stress is defined:

$$\sigma(t) = G^*(\omega)\gamma(t) \tag{2.18}$$

Using the 'generalized Maxwell' model found in equation (2.16), $G^*(\omega)$ is found to be:

$$G^*(\omega) = \sum_{i=1}^{n} \frac{i\omega\eta_i}{1 + i\omega\tau_i} \tag{2.19}$$

It is normal to write:

$$G^* = G' + iG'' \tag{2.20}$$

Where G' is called the storage modulus and is related to the elastic behavior and G'' is called the loss modulus and is related to the viscous behavior of the fluid. From equation (2.19) each of these modulus could be derived for the 'generalized Maxwell' model:

$$G' = \sum_{i=1}^{n} \frac{\omega^2 \eta_i \tau_i}{1 + \omega^2 \tau_i^2} \tag{2.21}$$

$$G'' = \sum_{i=1}^{n} \frac{\omega \eta_i}{1 + \omega^2 \tau_i^2} \tag{2.22}$$

If G'' is larger than G' the viscous behavior is dominant and the structure will be liquid-like. If G' is larger than G'' the elastic behavior is dominant and the structure will be solid-like. When the modulus's are equal it is defined to be at the gel point [5, 6]. These two modulus could be combined into what is called complex viscosity:

$$\eta^* = \eta' - i\eta'' = \frac{G'' - iG'}{\omega} \tag{2.23}$$

Here η' is called the dynamic viscosity and η'' have no name but is related to the dynamic rigidity. Often this is represented by the absolute value also called complex viscosity [5, 10]:

$$|\eta^*| = \frac{\sqrt{G'^2 + G''^2}}{\omega} \tag{2.24}$$

Experiments in rotational rheometer

Rheological properties are often investigated in a rheometer. A rheometer is an instrument that relies on rotation or oscillation of a rotor. Either in a cone-plate setup, shown in Figure 2.7, with a flat stationary plate and a rotating cone over, a parallel-plate setup with a flat plate substituting the cone or the coaxial setup with the sample placed between two cylinders, shown in Figure 2.8 [5, 7].

Two basic alternatives of measurements could be done in all geometries. Either controlled stress input (CS-rheometer) or controlled shear rate input (CR-rheometer). In each of this the other parameter is determined. The shear stress is related to the torque of the rotor and the shear rate is linked to the speed of the rotor. In addition there are two different designs related to how the stress and shear rate are measured. The Searle measuring system measure both the torque and the speed of the rotor on the rotor

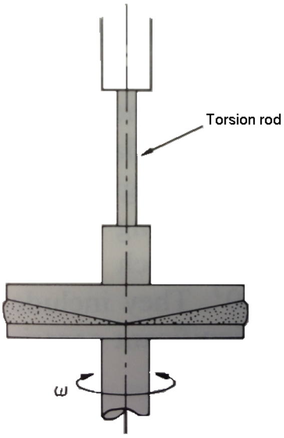

Figure 2.7: Schematic representation of a cone-and-plate rheometer. Figure adapted from [5].

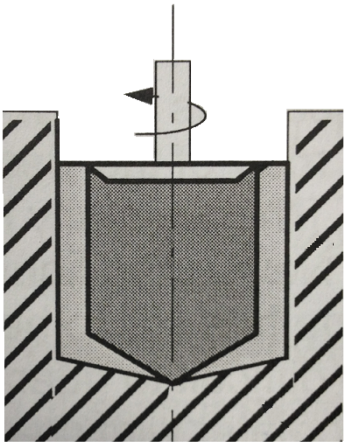

Figure 2.8: Schematic representation of a coaxial rheometer. Figure adapted from [7].

shaft axis. The Couette measuring system measure the torque on the rotor shaft axis while the speed is measured on the plate or the outer cup (coaxial rheometer) [5, 7].

Tests in rheometer could both be static and dynamic. Static tests involve the measuring of what happened when a step change in stress or strain and development in time after this change. Dynamic tests involve harmonically change in stress or strain and often are oscillatory movement used. Parameters that could be changed beside the stress or strain is frequency and time between each measurement. In many rheometers there are also possible to control the temperature and the pressure [5].

2.2 Sol-gel transition

The sol-gel transition is the transition from a solution(sol) state to an gel state. This take place because the dissolved medium starts formation of some macroscopic network. As mentioned in section 2.1 when talking about oscillatory shear the sol-gel transition could be measured in a rheometer and is when the storage modulus, G', is equal to the loss modulus, G''. A weak gel structure could be broken by shear and the best way to prevent this is by using small amplitude oscillatory measurements [11].

At the sol-gel transition the medium is neither a solution or a gel, but in a transition between them. It also could be characterized by divergency of the viscosity and appearance of elastic behavior. This behavior is shown in Figure 2.9 [12, 13].

The sol-gel transition could also be studied using different types of light scattering. In experiments using dynamic light scattering the sol-gel transition is recognized of the non-ergodic behavior by the correlation function [14]. Martin and Wilcoxon used quasielastic light scattering to measure the intensity function and the divergence in characteristic relaxation time at the gel-point [15, 16].

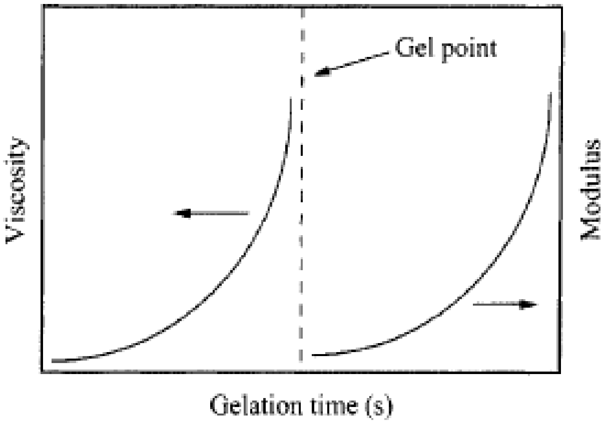

Figure 2.9: Schematic behavior of viscosity and modulus at the sol-gel transition. Figure adapted from [12].

2.3 Fracture mechanics

Fracture is a well known theory when it comes to linear elastic homogeneous solids. For heterogeneous materials it is more complicated. One should expect the most brittle places to crack first, but when you first have a crack this will contribute to how the stress gradient is in the material. This means that it is extremely statistical behavior for how fractures develop. Here it will be concentrated on the simplest, that is linear elastic fracture mechanics. Then nonlinear and dissipative process only is actual in a small volume around the crack tip called the fracture process zone or the failure zone. This is shown in Figure 2.10 [17, 18].

An ideal crack will start to propagate when the mechanical energy per unit area released by the solid, $\mathcal{G}$, is larger than the energy per unit area dissipated to create two new surfaces, Γ. The parameter Γ is often called the fracture energy. This is called the Griffith criterion as this is the criteria that must be fulfilled before the crack starts to propagate:

$$\mathcal{G} \geq \Gamma \tag{2.25}$$

Under quasi-static conditions, the crack velocity is as following:

$$\frac{1}{\mu} v = \mathcal{G} - \Gamma \tag{2.26}$$

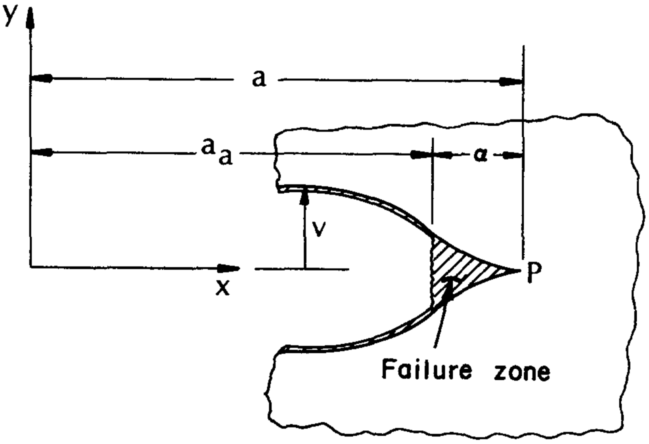

Figure 2.10: Cross-section of an ideal crack with the fracture process zone or failure zone marked. Figure adapted from [17].

Where μ is the effective mobility and v is the crack velocity. In general the fracture energy will depend on the entire history of stresses acting on the material. Experiments on the other hand shows that this is approximately constant. How the fracture develops depend on the crack velocity, the size of the failure zone, temperature, other environmental factors and on chemical aging effects. [17, 19, 20].

The largest speed a crack could have is equal to the Rayleigh wave speed, c_R, that is the velocity of an acoustic wave along the surface of the solid. As first approximation this would give the following [21]:

$$v = c_R \left(1 - \frac{\Gamma}{\mathcal{G}}\right) \tag{2.27}$$

Experimentally the speed of a crack seldom exceed half of this speed. This is because of the material reflecting elastic waves on the remote boundaries making the fracture unstable. This could also cause rougher fractures or branching [22].

2.3.1 Straight cracks

A straight crack in two dimensions is shown in Figure 2.11. Here σ_{ij} is the stress field, r is the distance to the crack tip and θ is the angle with respect to the crack. It is possible to have three different modes of fractures, the tensile mode (Mode I), the shearing mode (Mode II) and tearing mode (Mode III). These modes are shown in Figure 2.12 [21].

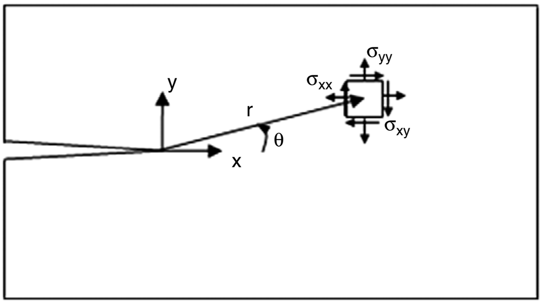

Figure 2.11: Sketch of an straight crack in a two-dimensional medium with the notation indicated. Figure adapted from [21].

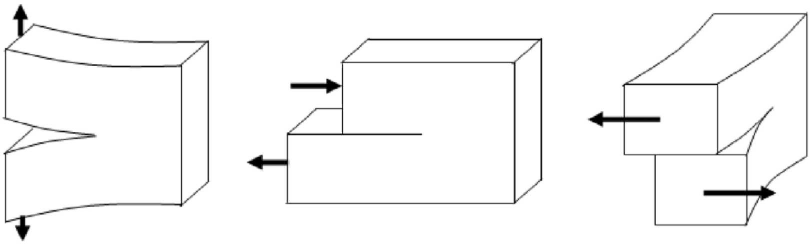

Figure 2.12: The three modes of fracture, respectively the tensile mode, the shearing mode and the tearing mode. Figure adapted from [21].

The stress field could approximately be written as follows:

$$\sigma_{ij} \approx \frac{1}{\sqrt{2\pi r}} \left(F_{ij}^{I}(\theta)K_I + F_{ij}^{II}(\theta)K_{II} + F_{ij}^{III}(\theta)K_{III} \right) \tag{2.28}$$

Here I, II and III comes from the different modes described. K is called the stress intensity factor and F_{ij} is a universal function. This means that it do not depend on the details of the crack, but on material properties and the angel θ. In most fracture process the Mode I is the dominant process and often the other two modes could be neglected. If the mechanical energy release per unit area is considered it could be shown that in a plane stress situation:

$$\mathcal{G} = \frac{K_I^2}{E} \tag{2.29}$$

Where E is the Young's modulus of the material. In plain strain conditions, the following will be the expression for the mechanical energy release per unit area:

$$\mathcal{G} = \frac{K_I^2}{E}\left(1+\nu\right) \tag{2.30}$$

Where E still is the Young's modulus and ν is the Poisson ratio of the material. K will rely on the length of the crack, the geometry of the sample and the applied tension. It could be explained that for an infinity large sample, K is proportional to the square root of the length of the crack [21].

2.4 Saffman–Taylor instability/Viscous fingering

In 1958 Saffman and Taylor studied the stability of the interface between two fluids with different viscosity. If the surface accelerate from the less viscous fluid towards the more viscous, the surface is unstable and viscous fingering appears. This is often called the Saffman–Taylor instability. The motion of the fluid is supposed to follow Darcy's law which was derived experimentally in 1855 [4, 23]:

$$\vec{u} = -\frac{k}{\eta}\nabla p = \nabla\phi \tag{2.31}$$

Where $\vec{u}$ is the velocity, k is the permeability, η is the viscosity, p is the pressure and ϕ is the velocity potential. Assuming the fluids are incompressible the equation of continuity is satisfied and this will give $\nabla\vec{u} = 0$ or $\nabla^2\phi = 0$ that is the Laplace's equation. An example from the classic experiment of Saffman and Taylor is shown in Figure 2.13

Saffman and Taylor assumed that the surface tension could be neglected and derived the following parametric equation for the surface of the finger:

$$x = \frac{w\left(1-\lambda\right)}{2\pi}\ln\left(\frac{1}{2}\left(1+\cos\frac{2\pi y}{\lambda w}\right)\right) \tag{2.32}$$

Where x is the direction the finger moves, y is in the direction of the width of the finger, perpendicular to x, w is the width of the cell and λ is the width

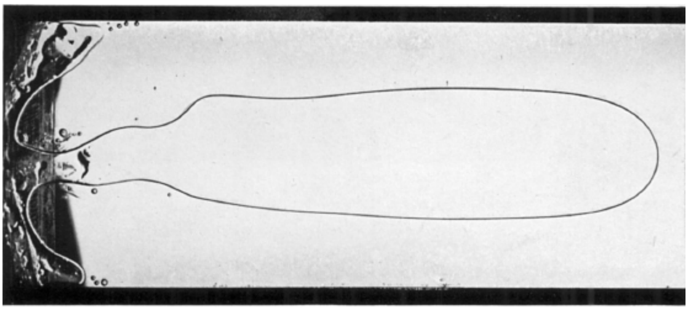

Figure 2.13: Picture of a viscous finger in a Hele–Shaw cell from the original work by Saffman and Taylor. Figure adapted from [4].

of the finger relative to the cell. In other words: $\lambda =$ (width of finger)$/w$. These parameters could be seen in Figure 2.14 with the origin taken at the tip of the finger. The parameter b is the gap between the plates. The experiments done by Saffman and Taylor indicated that λ will approach an asymptotic value of 0.5, which is said to be the limiting value for high velocities. This profile also fits equation (2.32) well for $\lambda = 0.5$, but not for other values of λ [4, 24, 25].

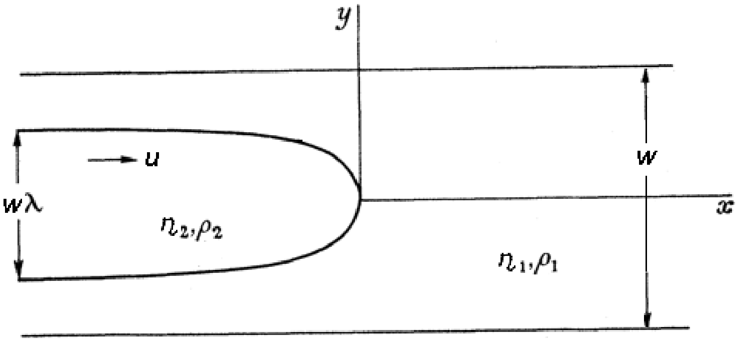

Figure 2.14: Parameters of a finger moving in a channel.

The assumption that the surface tension is negligible is found to be poor in many cases and the finger widens when this tensions becomes a more important contribution. It was proposed by Pitts in 1980 that λ is dependent on the capillary number, Ca, and the gap-width to cell-width ratio, ϵ, defined as:

$$Ca = \frac{\Delta\eta u}{\sigma} \tag{2.33}$$

$$\epsilon = \frac{b}{w} \tag{2.34}$$

Where $\Delta\eta$ is the difference in viscosity between the two fluids, u is the velocity of the finger and σ is the surface tension, this could then be fitted to the model. McLean and Saffman proposed in 1981 [26] the right scaling to be Ca/ϵ^2. This shows a good agreement with experimental results for some cases as shown by Park and Homsy in 1985. This scaling is often summed up in the factor $1/B$ and represent the ratio of viscous forces over the capillary forces [24, 27, 28, 29].

$$1/B = \frac{12Ca}{\epsilon^2} = \frac{12\eta u w^2}{\sigma b^2} \tag{2.35}$$

The function $\lambda(1/B)$ was first estimated numerical and in 1988 Rabaud et. al. [30] derived a function for this:

$$\lambda = \frac{\pi\alpha\sqrt{B}}{2}\left[\left(1 + \frac{4}{\pi\alpha\sqrt{B}}\right)^{1/2} - 1\right] \tag{2.36}$$

Where α is a proportionality constant found by the radius of curvature.

When a fluid is displaced by a less viscous fluid there is an instability which prevents a planar interface to occur. For a wide range of system parameters the interface between the fluids settle to a single finger. The surface tension, σ, is a very important factor and the instability could give a large response to even small noise [31, 32, 33]. Theoretical work have found that the values of λ seen experimentally is solutions of Darcy's law, but there is also many other solutions of the law that are not chosen. This selection is still a large question that still remain unanswered and understood physically [34].

Often other effects must be taking into account. That the interface is not straight but is forming a meniscus and the wetting-layer effect are two of them. In a more realistic model the fluid that is displaced will wet the walls, and leave a film behind that will complicate the boundary conditions. This is schematically shown in Figure 2.15. Park and Homsy proposed in 1984 [35] an effective surface tension to take care of this:

$$\sigma^* = \sigma\left(\frac{\pi}{4} + \alpha\lambda\left(w/b\right)\left(\eta u/\sigma\right)^{2/3}\right) \tag{2.37}$$

Where α, with reasonable values between 1.5 and 4, is related to the average of the normal to the interface with respect to the x-axis. This shows good agreement with experimental results except for large values of $1/B$ [26, 36, 37, 38].

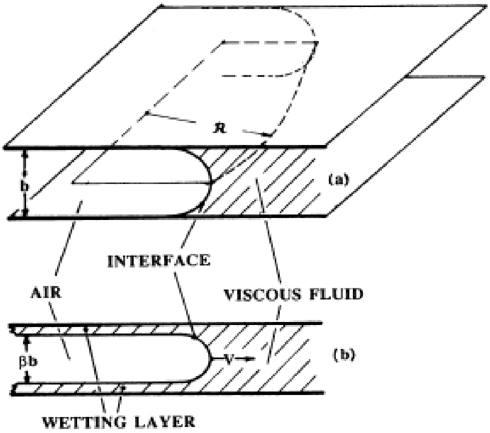

Figure 2.15: Schematics of the viscous finger (a) without and (b) with wetting-layer effect. Figure adapted from [39].

2.5 Fingering/Fracturing in a Hele-Shaw cell

The Hele–Shaw was invented by Henry Selby Hele-Shaw in 1898 [23]. It consists of two glass plates with a gap inbetween and is used to investigate viscous flow. To describe this flow Saffman and Taylor used Darcy's law, equation (2.31), with the permeability, $k = b^2/12$, where b is the gap between the plates, as an analogy for flow in porous media [4]. A sketch of an Hele-Shaw cell is shown in Figure 2.16.

The most usual experiment in the Hele-Shaw cell is to fill the cell with some viscous media and then use air or some other fluid to displace this media. Air have a viscosity of $1.82 \cdot 10^{-5}$ Pa·s and could be neglected in most experiments. How fluid-like or solid-like the response of the displaced media is given by the Deborah number, equation (2.5). It appears viscous fingers for $D_e << 1$, viscoelastic fractures for $D_e > 1$ and single plane

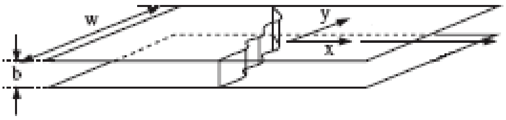

Figure 2.16: Sketch of an Hele-Shaw cell. Figure adapted from [40].

cracks for $D_e >> 1$. The differences is shown in Figure 2.17 [41, 42].

A Hele-Shaw cell could either be linear or radial and the difference is where the injection of displacing fluid takes place. If this is in the end of the cell, the cell is said to be linear, like shown in Figure 2.13. If the cell is radial the hole is in the middle and the pattern becomes like shown in Figure 2.17 and 2.18.

In addition the problem gets more complicated when the fluid is non-Newtonian. The instability could be described by a velocity dependency of the surface tension and the viscosity. The width of the finger could also be used to determine material properties by measuring the width of the finger. If the fluid is shear thinning the viscosity, that is a part of the $1/B$ parameter, is depending on the shear rate. For a weak shear thinning fluid it is sufficient to replace the viscosity η with $\eta(\dot{\gamma})$.

Lindner et. al. [25] found that the parameter α in the equation for $\lambda(1/B)$, equation (2.36) is linearly dependent on the factor n from Ostwald de Waele equation, equation (2.6) with the following equation:

$$\alpha = 4.29n \tag{2.38}$$

In the Hele-Shaw cell the shear rate could be approximated to be:

$$\dot{\gamma} \approx \frac{u}{b} \tag{2.39}$$

Where u is the finger velocity and b is the gap between the plates.

For stronger shear thinning fluids Darcy's law must be rewritten to find the dependency in the pressure gradient and in some cases the normal force,

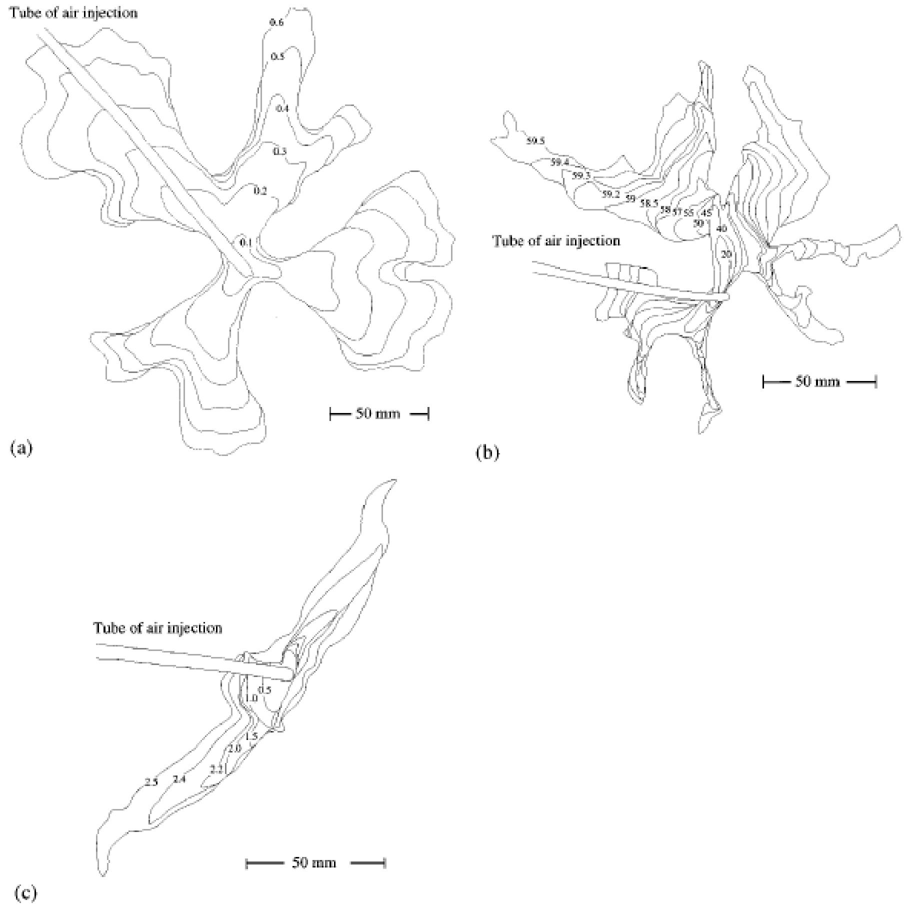

Figure 2.17: Overview of different patterns obtained in a radial Hele-Shaw cell. In (a) viscous fingering, (b) viscoelastic fracturing and (c) single plane cracking. Figure adapted from [41].

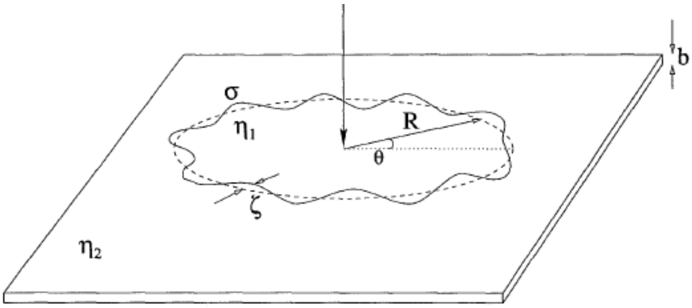

Figure 2.18: Schematics of an radial Hele-Shaw cell. Figure adapted from [43].

$N_1(\dot{\gamma})$ also must be included in a effective surface tension:

$$\sigma^* = \sigma + \frac{1}{2} N_1(\dot{\gamma}) b \tag{2.40}$$

With the right corrections to the $1/B$ factor the curve of experimental results shows good agreement of the classical curve for $\lambda(1/B)$. In other complex fluids with higher Deborah number and a more elastic response this will be even more complicated and λ get irrelevant as the patterns appears more fracture like. [25, 41, 44, 45, 46].

2.6 Polarization and birefringence

Light could be seen on as electromagnetic waves described by Maxwell's equations:

$$\nabla \cdot \boldsymbol{E} = \frac{1}{\epsilon_0} \rho \tag{2.41}$$

$$\nabla \cdot \boldsymbol{B} = 0 \tag{2.42}$$

$$\nabla \times \boldsymbol{E} = -\frac{\partial \boldsymbol{B}}{\partial t} \tag{2.43}$$

$$\nabla \times \boldsymbol{B} = \mu_0 \boldsymbol{J} + \mu_0 \epsilon_0 \frac{\partial \boldsymbol{E}}{\partial t} \tag{2.44}$$

Where $\boldsymbol{E}$ is the electric field vector, $\boldsymbol{B}$ is the magnetic field vector, ρ is the charge density, $\boldsymbol{J}$ is the volume current density vector and ϵ_0 and μ_0 is respectively the permittivity and the permeability of free space.

In free space, ρ and $\boldsymbol{J}$ are zero and it could be shown that the wave has no electric field in the direction the light propagates. If the light propagate in the x-direction and the electric field is in the y-direction it could be shown that:

$$E_y = cB_z \tag{2.45}$$

The magnetic field is normal to both the direction the light propagate and the electric field. In size the magnetic field only differs from the electric with a scalar. This is shown in Figure 2.19 [47, 48].

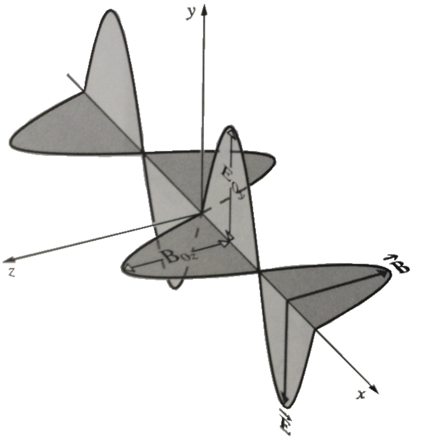

Figure 2.19: Schematic of E-field and B-field of light. Figure adapted from [47].

The moment-by-moment direction of the E-field is defined as the polarization. In Figure 2.19 the E-field is only in the xy-plane. This corresponds to linearly polarized light. It could be described by the following equation for a harmonic wave.

$$E_y(x,t) = E_{0y}\cos(kx - \omega t) \tag{2.46}$$

$$B_z(x,t) = B_{0z}\cos(kx - \omega t) \tag{2.47}$$

Where E_{0y} and B_{0z} is the amplitude of the wave. Light could also have other polarization like elliptical or circular. In these cases the polarization will change direction. In Figure 2.20 circular polarization is shown [47, 48].

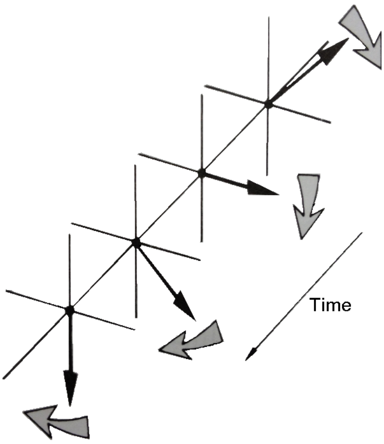

Figure 2.20: Circular polarized light. Figure adapted from [47].

2.6.1 Birefringence

In free space an electromagnetic wave propagates with the speed $c = 1/\sqrt{\epsilon_0\mu_0} = 3 \cdot 10^8$ m/s. In a medium on the other hand an electromagnetic wave propagate with a speed $v = 1/\sqrt{\epsilon\mu}$ that is slower than c. Here ϵ and μ is the permittivity and the permeability of the medium. The ratio of the speed in free space over the speed in the medium is defined as the absolute index of refraction, n:

$$n = \frac{c}{v} = \sqrt{\frac{\epsilon\mu}{\epsilon_0\mu_0}} \tag{2.48}$$

In many substances the optical properties are anisotropic. This means that the index of refraction is different for various directions in the substance. This could be described by two indexes called the ordinary, n_o, and the extraordinary, n_e, refractive index. Here the extraordinary is defined to be parallel to the axis of anisotropy and the ordinary is perpendicular to this. The difference in these indexes are a measure of the birefringence:

$$\Delta n = n_e - n_o \tag{2.49}$$

One way to observe the birefringence in a sample is to use crossed polarizers. White light will go through a linear polarizer, then the sample and then another linear polarizers axis perpendicular to the first polarizer. If the sample is optical isotropic no light will go through the second polarizer. So if light could be seen going through the second polarizer it is because the sample shows birefringence. This is shown in Figure 2.21 [47, 49].

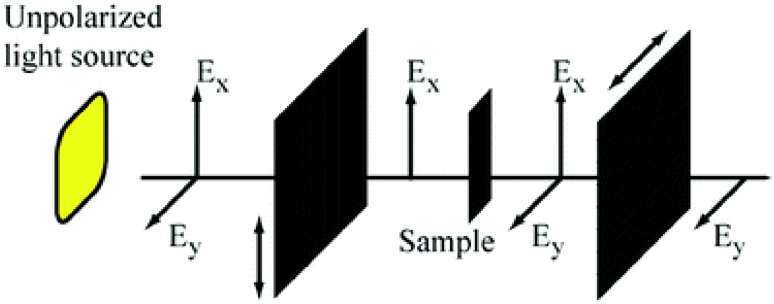

Figure 2.21: Example of setup used when observing birefringence in the sample. Figure adapted from [49].

Nematic phase

Crystals always have a perfect structure with a preferred direction and is not orientation dependent. On the other hand liquids are completely isotropic. There are some molecules that spontaneously could obtain an inner ordering in the liquid phase and make some anisotropy. These are called liquid crystals or nematogens. The phase is called nematic. The nematic phase shows a directional order, but no positional order. If there also is a positional order it is called a smectic phase. This is described in Figure 2.22 [50].

The nematic director, $\boldsymbol{n}$, describes the preferred direction of the nematogens and is along the optical axis. The nematic phase have the property $\boldsymbol{n} = -\boldsymbol{n}$, so turning the system 180° will give the same optical properties. How aligned the nematogens are is described by the nematic order parameter, S_2:

$$S_2 = \left\langle \frac{3\cos^2\theta - 1}{2} \right\rangle \tag{2.50}$$

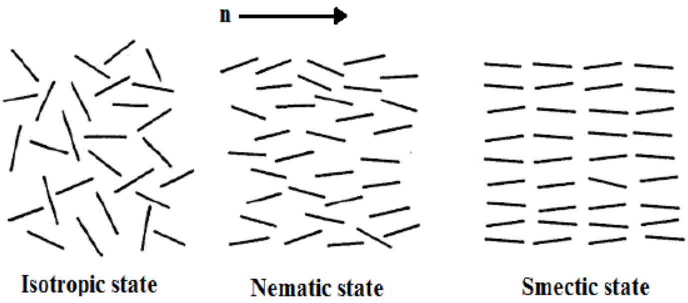

Figure 2.22: Illustration of microscopic structure and order of the isotropic, nematic and smectic phase. Figure adapted from [51].

Here θ is the angel between each individual nematogen to the nematic director. $S_2 = 0$ for an isotropic distribution and $S_2 = 1$ for a perfect orientation. S_2 is also proportional to the birefringence Δn [50, 52].

2.6.2 Polarizers and quarter-wave plate

Normal white light contains light with all polarizations. An optical device that could take unpolarized light as input and send out polarized light is called a polarizer. A linear polarizer for example will transmit only light with polarization along one axis and block light with other polarizations as seen in Figure 2.23 [47].

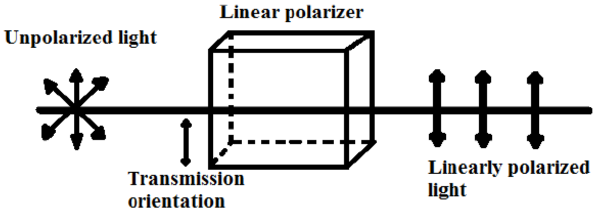

Figure 2.23: The basic principle of a linear polarizer. Unpolarized light enters the polarizer and only light with linear polarization along one plane is transmitted. Figure adapted from [1].

A quarter-wave plate is an optical device that introduce a relative phase shift of 90° between the ordinary and the extraordinary axis. This gives that linear polarized light get transferred into circular or elliptical polarized light [47].

Mathematical description

Mathematically polarization of light could be described by Stokes vectors. This is a column vector with four elements, each describing one type of polarization. The Stokes vector for 45° linear polarized light is:

$$\begin{pmatrix}1\\0\\1\\0\end{pmatrix}$$

And for right-handed circular polarized light the Stokes vector is:

$$\begin{pmatrix}1\\0\\0\\1\end{pmatrix}$$

Every optical device like polarizers and wave plates that transmit light could then be described by a 4×4 Mueller matrix. If a Stokes vector is multiplied with a Mueller matrix a new Stokes vector describing the polarization of the outgoing light is obtained. For example the Mueller matrix for a quarter wave plate with fast vertical axis is:

$$\begin{pmatrix}1&0&0&0\\0&1&0&0\\0&0&0&-1\\0&0&1&0\end{pmatrix}$$

If initial 45° linear polarized light goes through a quarter-wave plate with fast vertical axis the calculation gives circular polarized light out as expected [47]:

$$\begin{pmatrix}1&0&0&0\\0&1&0&0\\0&0&0&-1\\0&0&1&0\end{pmatrix}\begin{pmatrix}1\\0\\1\\0\end{pmatrix}=\begin{pmatrix}1\\0\\0\\1\end{pmatrix}$$

2.7 Clay minerals

Clay minerals can be found everywhere on earth and have since ancient time been used in art, building material etc. Natural clay is a very heterogeneous mixture of minerals, but pure clay could also be made synthetically. The term clay is used only for natural clay, but clay mineral can be both natural and synthetic. This will be used throughout this thesis [53, 54, 55].

Clay contains layers of sheets and each sheet is either tetrahedral or octahedral. The difference between this could be seen in Figure 2.24. Further clay minerals are classified in either 1:1 or 2:1 structure. Here 1:1 means one layer contains one tetrahedral and one octahedral sheet, and 2:1 means that one layer contains one octahedral sheet between two tetrahedral sheet [53]. This is shown in Figure 2.25.

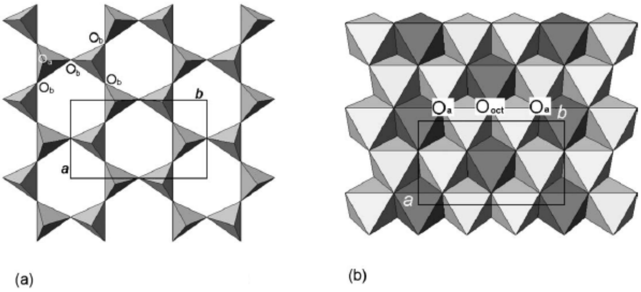

Figure 2.24: (a) an tetrahedral sheet and (b) an octahedral sheet of clay minerals. Figure adapted from [53].

The 1:1 layer structure is more compact than the 2:1 layer structure. This have the interlayer distance $d_{001} \sim 7$ Å while for an empty 2:1 structure $d_{001} \sim 9$ Å. 2:1 layer structures often have a negative surface charge and then it can be cations between the layers. In almost every clay mineral there is intercalated water between layers in normal humidity and temperature. Clay minerals will react different in form of the number of water layers intercalated. When some clay minerals are dissolved in water they will swell and completely exfoliate. In this thesis a 2:1 smectic, swelling clay mineral called laponite is used. This is one of the most widely studied synthetic clay minerals, and in addition it is transparent when dissolved in water so it is easy to see through it when it is in the Hele-Shaw cell. In Figure 2.26

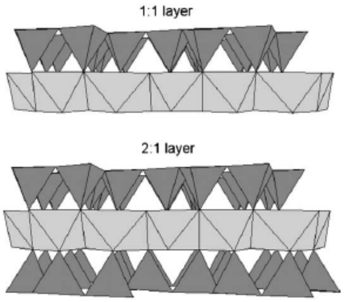

Figure 2.25: Difference of an 1:1 and 2:1 layered clay mineral. Figure adapted from [53].

a overview of a typical 2:1 smectic clay mineral is found [53, 55, 56].

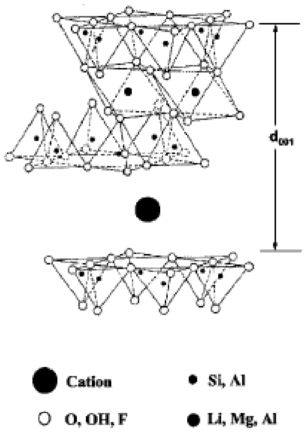

Figure 2.26: Structure of a typical 2:1 layered clay mineral. Figure adapted from [57].

2.7.1 Laponite

As mentioned, laponite is a 2:1 smectic clay mineral and the empirical chemical formula is $Na^{0.7+}[Si_8Mg_{5.5}Li_{0.3}O_{20}(OH)_4]^{0.7-}$, where Na is a interlayer cation that can be changed. The layers are almost round with a diameter of 25 nm and the thickness of one platelet is 0.92 nm. The surface charge of the platelets is negative and on the edge there is a smaller positive charge.

A schematic figure of a laponite platelet is shown in Figure 2.27 [58].

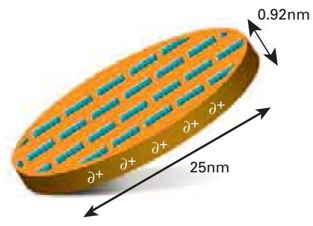

Figure 2.27: Schematics of a laponite platelet. Figure adapted from [58].

In experiments performed during this thesis, laponite is dispersed in water or a NaCl solution. If dispersing in distilled water the ionic strength is less than 10^{-4} mol/L. When dispersing in water laponite delaminate into almost only single platelets, but to shear melt all structures it must be subjected to strong shear. Stress over about 9 Pa will start to destroy structures. Scattering experiments have shown that filtering will destroy almost all existing structures, but the filtering have no influence of rheological properties [10, 59, 60, 61].

Laponite is a interesting material because it have several final arrested states with different concentration of clay mineral and ions. The first trial to make a phase diagram was done by Mourchid et. al. in 1995 [62]. Later more studies on this have been done and there are still some disagreements on the phase diagram. The phase diagram with respect to concentration of salt and laponite is shown in Figure 2.28. The different arrested states that have been reported are gel, repulsive (Wigner) glass and attractive glass. The repulsive glass is formed by long-range Coulomb interaction while the attractive glass and gel are formed by van der Waals attractions. For higher ionic strength than 10^{-2} M flocculation will occur. [63, 64, 65, 66, 67].

The Coulomb interaction represent a fast process. For high concentrations of clay mineral and low ionic concentration the arrested state will be a repulsive glass. For lower concentrations of clay mineral the process become slower because van der Waals attraction must make some clusters before the repulsive forces could form a solid. For higher concentration of ions the Coulomb interaction is screened and the attractive forces are dominant and will make a attractive glass or gel. The difference between these two are

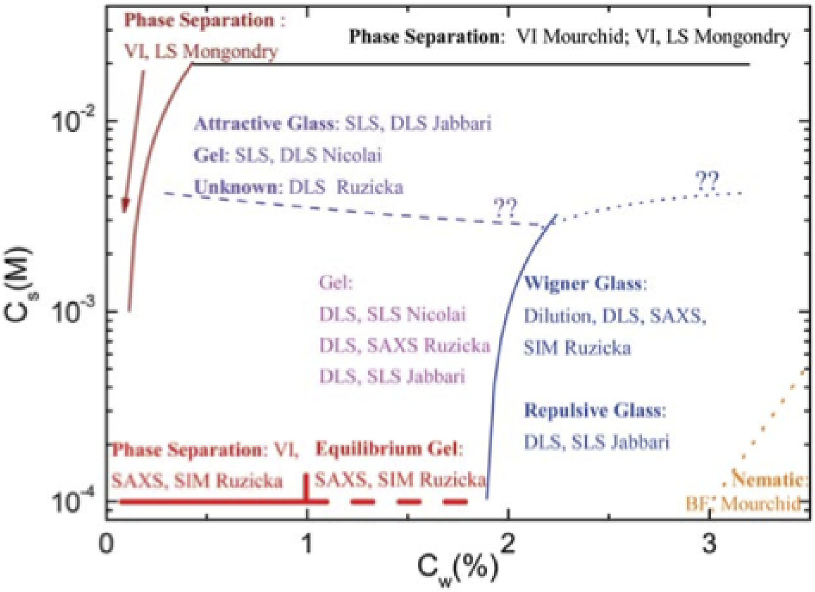

Figure 2.28: Phase diagram of laponite. C_w is the weight percent of laponite and C_s is the concentration of NaCl in mol/L. Figure adapted from [67].

that the attractive glass have a homogenous structure while the gel is heterogenous. Controlling the pH or/and the conductivity of the initial sample can be important to know exactly the ionic strength [56, 61, 65, 68, 69].

There are basically two different possibilities platelets of laponite can stick together. Either with a T-shape or with the overlapping coins configuration. This is shown in Figure 2.29. In the energy spectrum the T-shape have a broad minimum while the overlapping coins will have a deeper and narrower minimum. For ionic strength bellow $5{\cdot}10^{-3}$ the forces are mainly repulsive, but from this concentration the overlapping coins are the preferred configuration although T-shape also is found. An aging effect with the change from T-shape to overlapping coins is found although the sample show solid behavior [70, 71].

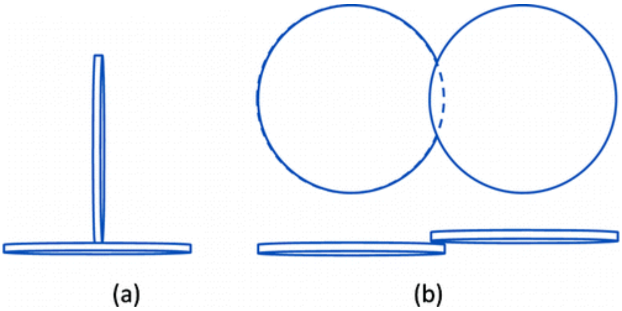

Figure 2.29: Different possible edge to surface interactions of laponite. (a) T-shape and (b) overlapping coins. Figure adapted from [71].

For clay concentration under 3 wt%, and on a short time-scale laponite will appear as a liquid and the rheological behavior will be Newtonian. For higher concentration and longer waiting time it will behave shear thinning and have a yield stress that must be overcome before it flows. The Herschel-Bulkley model is a good approximation of this. Laponite also show a aging effect and structures are broken if they are exposed for high stresses. This thixotropic behavior is difficult to model but needs to be taken into account in experiments with laponite [9, 72, 73].

Chapter 3

Experimental

3.1 The Hele–Shaw cell

The cell was developed through my ninth semester project and during the master thesis four cells have been used. The parts to the cell was made on the mechanical workshop at NTNU.

A sketch of the cell is shown in Figure 3.1 and a picture of the cell is shown in Figure 3.2. Both glass plates are 8 mm thick, the spacer fix the gap to 2.1 mm and the width of the cell/pistons are 100 mm. The gap-width to cell-width ratio is given by equation (2.34) to be: $\epsilon = 2.1/100 = 0.021$. The gap is so small that the flow is assumed to be two-dimensional. The hole in the middle has a diameter of 5 mm.

The whole cell except the pistons are made of aluminum. The pistons are made of inox steel and have a height of 2 mm that is smaller than the gap. To make the cell water-proof it is made four wells at the end of the pistons and these are filled with joints of Gore-Tex. This could be seen in Figure 3.3. The cell is attached to the rack and the height is adjusted to the motors and the whole cell is leveled.

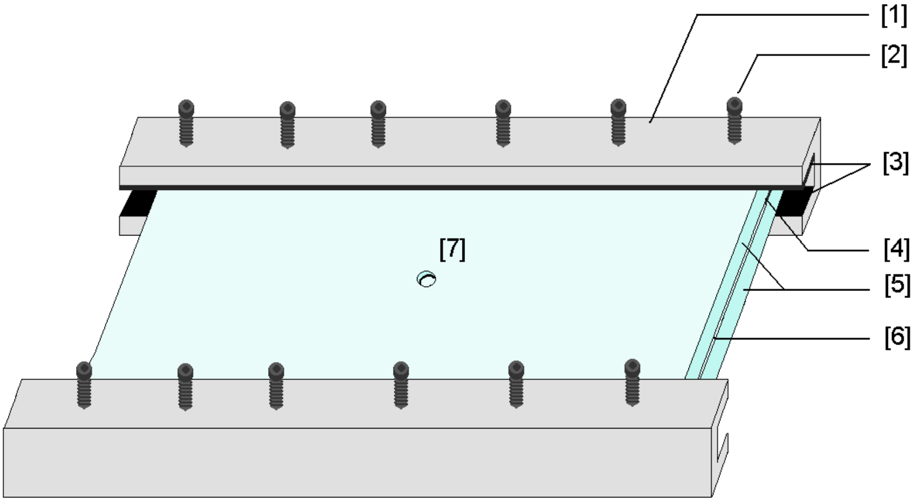

Figure 3.1: Sketch of the Hele-Shaw cell. Here [1] is the holder that the glass plates and spacer is put into, [2] is the screws that is used to hold the cell completely together, [3] is rubber to protect the glass, [4] is the spacer that fix the gap between the plates, [5] is the glass plates, [6] is the gap where the pistons are inserted and [7] is the hole to inject clay and air during experiments.

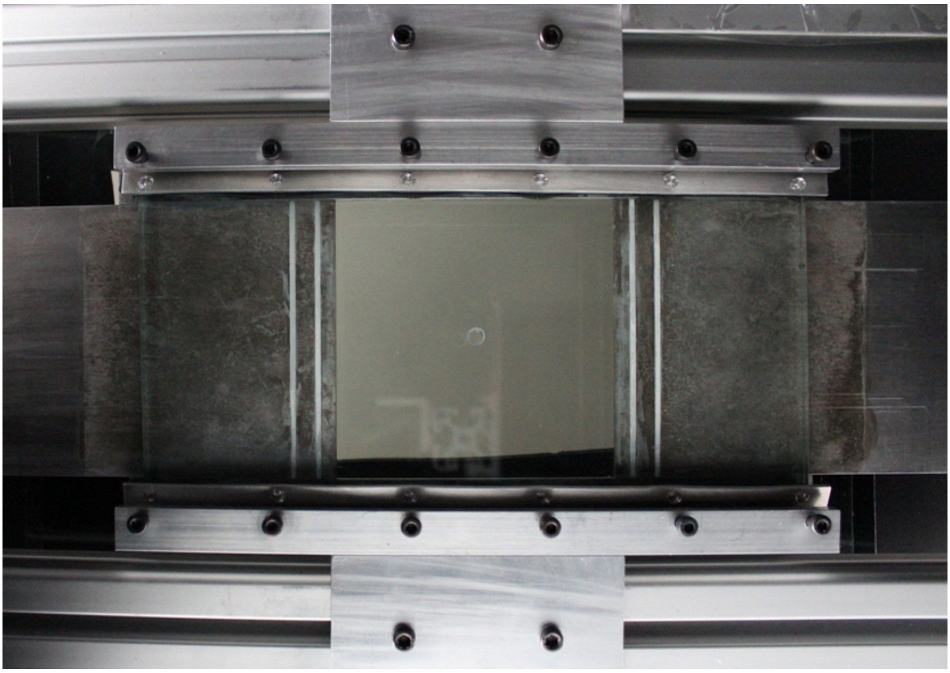

Figure 3.2: Picture of the Hele-Shaw cell.

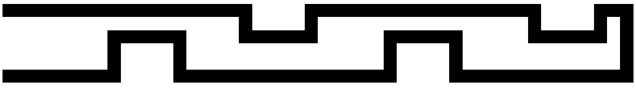

Figure 3.3: Sketch of the wells on the pistons that is filled with joints of Gore-Tex.

3.2 Preparation of clay samples

The clay mineral used in this thesis is laponite RD and is purchased from Laporte Ltd [58]. The concentration used is 3.0 wt% laponite and 97 wt% distilled water or NaCl solution. More about laponite could be found in section 2.7.1. All preparation is performed in room-temperature, 23° Celsius, and in a N_2 environment inside a glove bag. The laponite is dried in a oven at 170° Celsius for 24 hours before weighted and added bit by bit to the distilled water or NaCl solution while stirring with an magnetic stirrer. The laponite clay suspension is stirred for 30 minutes before filtered through a filter with 0.8 micrometer pore size to make a reproducible initial state with the laponite uniformly dissolved.

3.3 Experiments in the Hele-Shaw cell

The experiments done during this thesis was performed in the Hele-Shaw cell shown in Figure 3.2. The pistons can be pulled apart causing a finger/fracture to develop from the center hole of the cell. The motors that move the pistons are controlled by the computer software 'Venus1Term'. This is described in appendix B. Under the cell there is a light source to see the patterns in the cell better. The light source produce heat and is only turned on during the experiment to prevent temperature effects.

In this thesis the laponite suspension is studied in the liquid state, throughout the sol-gel transition and in the solid state. A start distance between the pistons of 100 mm is used that gives an aspect ratio of 1. Samples is mixed with distilled water or a NaCl solution with concentration up to 10^{-2} M. Higher NaCl concentration decreases the gelling time dramatically, but also make another final arrested state, see the phase diagram in Figure 2.28.

It is important when injecting the clay through the hole to prevent air bubbles because this will interact with the finger/fracture. The clay suspension is left in the cell for a desired amount of time. In the experiment done during this master thesis waiting time, τ_w, from 0 hours up to 606 hours is used. A camera is used to record the experiment. This is described in appendix C.

Other parameters that could be changed is the velocity of the pistons and the ratio and height of the cell. In this thesis this is not considered and the velocity is held constant at 0.2 mm/s, the aspect ratio (length between piston/width of cell) have been 1.0 and the height have been 2.1 mm for all experiments. Some experiments are done using crossed polarizers to see nematic phases in the clay suspension both before, under and after the experiment. In addition a few experiment have been done using tracer particles to see flow in the bulk of the clay.

3.3.1 Experiments with crossed linear polarizer

An overview of the experiment when using crossed linear polarizers is shown in Figure 3.4. Here unpolarized light is polarized with a linear polarizer and sent through the sample and then through a second polarizer with principal axis normal to the first polarizer. If the sample is homogenous no light will let through the last polarizer, but if the sample contains a nematic phase the sample will change the polarization and the change will go through the second polarizer. For more about polarizers see section 2.6.2

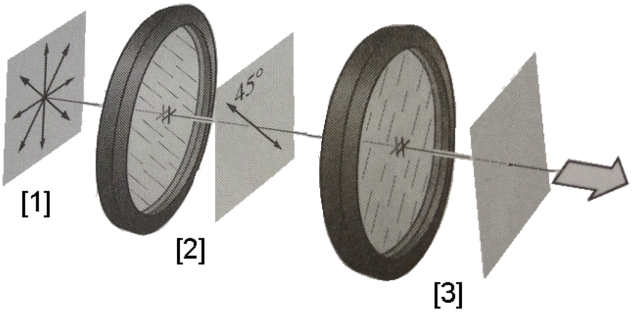

Figure 3.4: Overview of the setup using crossed linear polarizers. Here [1] is the initial unpolarized light, [2] is the the linear polarized light after passed the first polarizer. Here is the sample inserted, [3] is the light after passing the second linear polarizer with principal axis normal to the first one. If the sample have not changed the polarization no light will be let through this polarizer.

3.3.2 Experiments with crossed circular polarizer

An overview of the experiment when using circular polarized light is shown in Figure 3.5. The principle is the same as with linear polarizer, but here circular polarized light is sent through the sample. If the sample is homogenous the polarization will not change and no light will let through the setup. A nematic phase will change the polarization to some elliptical polarization that is not blocked by the last linear polarizer.

To produce circular polarized light the light is first let through a linear polarizer and then through a quarter-wave plate with principal axis 45° to the polarizer. After going through the sample the light will pass a new quarter-wave plate that will make circular polarized light into linear polarized light. Then the light pass through a linear polarizer that will block this light so only the change in polarization caused by the birefringence of the sample go through the last polarizer.

The quarter-wave plate only function good in a small range of wavelength of light and therefore it is used a filter that only let light with wavelength over 600 nm through. The measurement of the quarter-wave plate is showed in section 4.1.

3.3.3 Experiments with tracer particles

To better understand the movement in the bulk of the sample a few experiments are performed using silver nanoparticles with a size of 20.30 micrometer. The particles are shaken into the sample after filtration with a concentration of around 1 g/L before filled into the cell. The experiments are performed without polarizers, but the final state after the experiment is investigated with crossed polarizers. This is to get a better understanding of the context between the experiments performed with polarizers.

3.4 Rheology experiments

To check rheological properties of laponite, a Physica MCR300 Rheometer from Anton Paar is used. A picture of this is shown in Figure 3.6. This

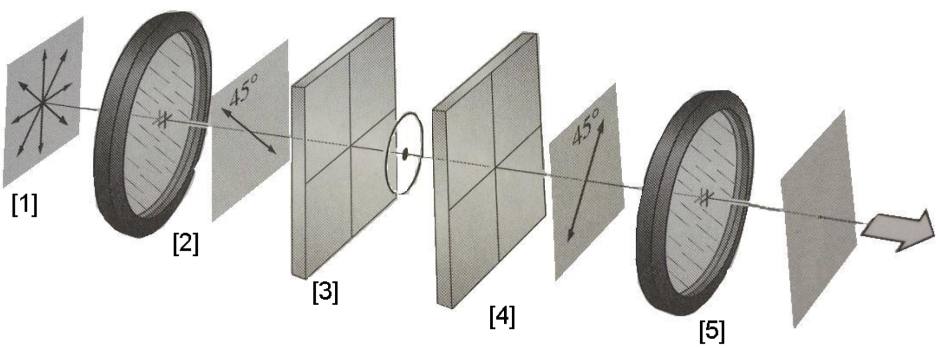

Figure 3.5: Overview of the setup using circular polarized light. Here [1] is the initial unpolarized light, [2] is the linear polarized light after passing the first polarizer. [3] is a quarter-wave plate with principal axis 45° to the first linear polarizer that will make the light circular polarized. Here is the sample inserted. [4] is the second quarter-wave plate that will change the polarization back to linear if the sample have not changed the polarization. [5] is the light after passing the second linear polarizer with principal axis 45° to the second quarter wave plate. If the sample have not changed the polarization no light will be let through this polarizer.

rheometer has a Searle measuring system and could be used both in CS and in CR mode. More about rheometers is found in section 2.1.2.

For experiments performed in the rheometer during this thesis the CR mode are used with a coaxial setup and oscillatory measurements. The shear rate is set to 0.5 %, the frequency is set to 0.1 Hz and the experiment is performed in room temperature, 23° Celsius. After the clay is prepared 20 mL is filled into the cylinder and covered with silicon oil to prevent evaporation. Then the experiment is started after different waiting time to check if the measurement it self will have influence on the gelling time.

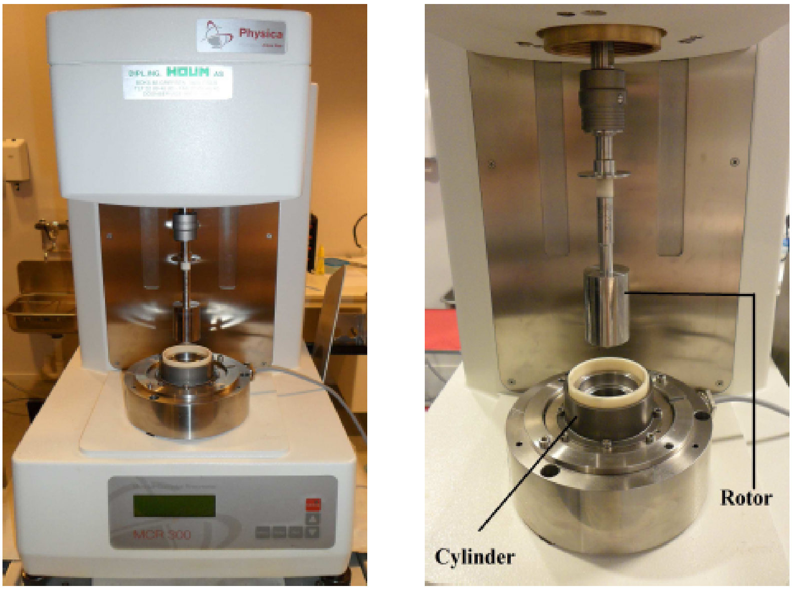

(a) *An overview of the rheometer.*

(b) *Zoom in of the rheometer, showing the rotor and the cylinder.*

Figure 3.6: The Physica MCR300 Rheometer. Figure adapted from [1].

Chapter 4

Results and discussion

4.1 Optical experiment on quarter-wave plate

With help of an ellipsometer the Mueller matrix of the quarter-wave plate is measured. The result is shown in Figure 4.1. In section 2.6.2 the theoretical matrix is found. The critical here is the large deviation in element MM_{33}, MM_{34}, MM_{43} and MM_{44}. It is only for high frequencies in the visible range (red light) that the quarter-wave plate works. For low frequencies (violet and blue light) it almost works as a half-wave plate and this will give a large uncertainty if the whole spectrum of light is used. In experiments performed using the quarter-wave plate the light pas through a filter with cutoff-frequency 600 nm.

4.2 Experiments done in the Hele-Shaw cell

In this thesis all experiments are performed using 3.0 wt% laponite with velocity 0.2 mm/s of the pistons, $\epsilon = 0.021$ and aspect ratio of 1.0. In each experiment the initial state is a small bubble just outside the hole in the glass plate. The clay is dissolved in distilled water or a NaCl solution with concentrations up to 10^{-2} M and the experiments are performed after different waiting times up to 606 hours. The only changing parameter is the NaCl concentration and the waiting time. As these parameters change it is observed four different patterns of the air bubble; viscous fingers, smooth

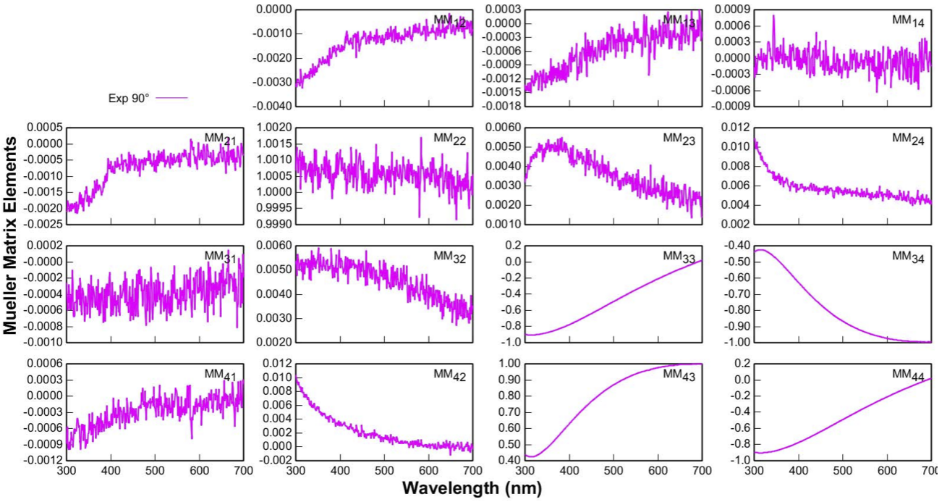

Figure 4.1: Experimental found Mueller matrix of the quarter-wave plate.

X-shapes, asymmetric and rough shapes and fractures. Each of these are described in the following sections.

4.2.1 Viscous fingers

Experiments done observing viscous fingering is for low NaCl concentration and short waiting time. An example with distilled water and waiting time 30 hours is shown in Figure 4.2. Viscous fingers are characterized with symmetry and have no rough edges. First it develops like a perfect bubble before it extends in the direction of the pistons and become a elongated Newtonian finger. This is on a short waiting time before the clay starts to gel. To have a perfect symmetric shape the cell have to be exactly leveled.

4.2.2 X-shapes

For longer waiting times a symmetric, smooth X-shape develops as seen in Figure 4.3. This could be linked to the fact that the viscosity of laponite follows the Herschel-Bulkley fluid model with a shear thinning behavior. In the start of the experiment the velocity of the finger is largest and the shear rate is linearly dependent on the finger velocity. According to the

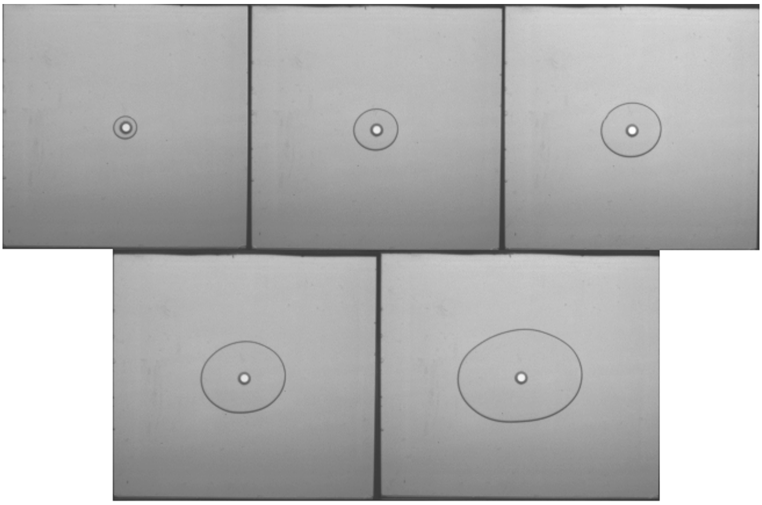

Figure 4.2: Experiment in Hele-Shaw cell with $C_s = 0$ and $\tau_w = 30{:}00$ h. The first picture is of the initial condition and then the pictures are after 6, 15, 30 and 60 seconds.

Herschel-Bulkley fluid model the viscosity is largest during the start of the experiment and so are the parameter $1/B$. This will give a small λ. As the experiment goes further the velocity of the finger will decrease and the parameter $1/B$ will be smaller. This will cause a wider finger. The splitting at the end could be explained by the boundary condition when the finger comes closer to the piston.

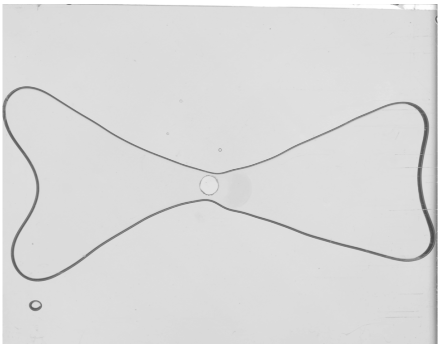

Figure 4.3: Experiment in Hele-Shaw cell with $C_s = 10^{-3}$ and $\tau_w = 11{:}00$ h. The picture are after 60 seconds from the start of the experiment.

4.2.3 Asymmetric and rough shapes

For even longer waiting times and higher NaCl solution a more asymmetric and rough shape is observed. For the shortest waiting time the observed pattern is almost round like a bubble but with some disturbance along the interface. For longer waiting times the pattern gets more and more rough along the interface. This is shown in Figure 4.4. These rougher shapes that are observed is linked to elastic behavior, so the sample is viscoelastic. As the waiting time increase the pattern gets rougher and rougher.

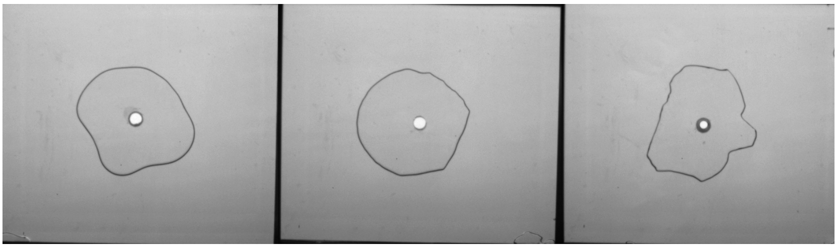

Figure 4.4: Experiment in Hele-Shaw cell with $C_s = 0$ and $\tau_w = 66{:}50$ h, $\tau_w = 90{:}00$ h and $\tau_w = 161{:}40$ h. The picture are after 60 seconds from the start of the experiment.

4.2.4 Fractures

For high salt concentration and long waiting time fractures are observed. This is shown in Figure 4.5. Pure elastic behavior is observed and the sample could be considered to be solid. Ideally the fracture should be normal to the direction the pistons move, but this is seldom seen. Also three fractures propagating from the initial bubble are observed. These two effects is discussed in section 4.7.3.

4.2.5 Phase diagram

The experiment done in this thesis is presented in the phase diagram found in Figure 4.6. Here the different shapes described over is indicated. Two lines also separates the liquid behavior, the viscoelastic behavior and the solid behavior.

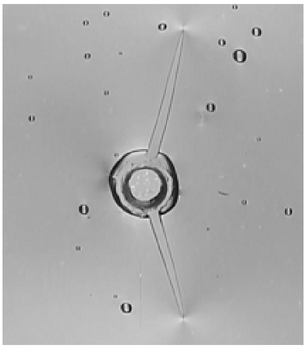

Figure 4.5: Close up of an experiment in Hele-Shaw cell with $C_s = 9.5 \cdot 10^{-3}$ and $\tau_w = 140{:}40$ h. The picture are after 1 second from the start of the experiment.

This phase diagram indicating the size of the Deborah number. For the liquid phase $D_e << 1$, for the viscoelastic phase $D_e > 1$ and for the solid phase $D_e >> 1$.

4.3 Experiments in Hele-Shaw cell with crossed polarizers

Crossed polarizers will show if there are alignments that will give birefringence in the clay. For the different phases described in the previous section different patterns of birefringence are observed. Birefringence have been investigated using crossed linear polarizers, with different direction of the axis, and with circular polarization.

4.3.1 Liquid behavior

In the liquid phase no birefringence is observed in the bulk of the material. As the finger propagate some birefringence is observed in front of the finger movement, but disappears. When the finger approach the pistons birefringence is seen between the finger and the piston. This is shown in Figure 4.7. As the movement stops this birefringence is conserved, but this is not a stable nematic phase that will be destroyed if applying stress again.

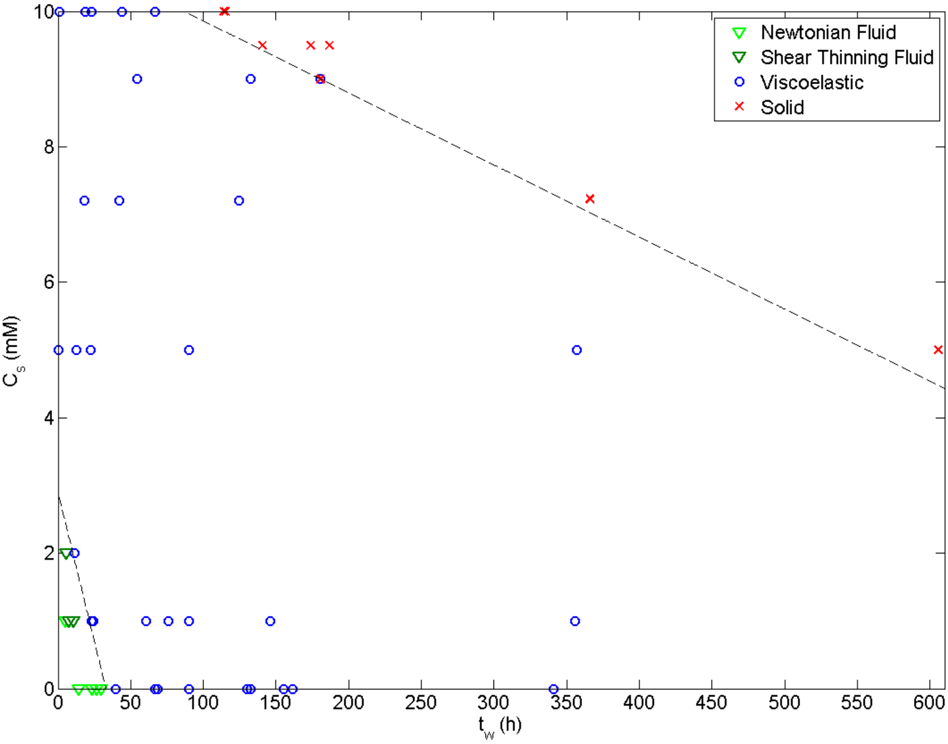

Figure 4.6: Phase diagram for 3 wt% laponite.

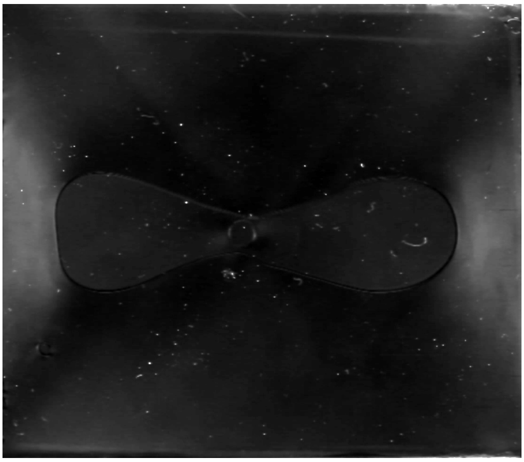

Figure 4.7: Experiment in Hele-Shaw cell with $C_s = 10^{-3}$ and $\tau_w = 10{:}50$ h. The experiment is with linear polarizers in the liquid phase (shear thinning).

4.3.2 Solid behavior

Figure 4.5 shows a experiment in the solid phase with circular polarization. Birefringence is only observed in a small area around the tip of the fracture. This birefringence will propagate along the fracture tip until the fracture reach the edge of the cell and disappears.

4.3.3 Viscoelastic behavior

In the viscoelastic phase different behavior is observed from how viscous-like or solid-like the sample is. In experiments done near the liquid phase, where the bubble is almost round, the birefringence is seen homogenous all around the bubble. For experiments done in more elastic clay the birefringence still is all around the rough bubble, but here patterns that look like fractures appears in the nematic phase. This is shown in Figure 4.8.

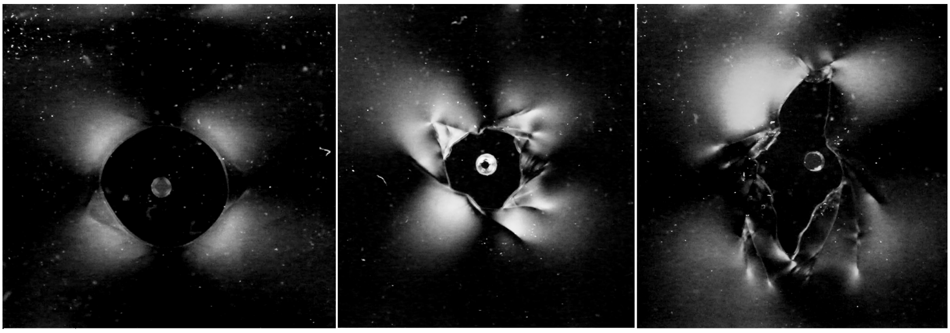

Figure 4.8: Experiment in Hele-Shaw cell with $C_s = 10^{-3}$ and τ_w = 22:50 h, τ_w = 90:10 h and τ_w = 146:10 h. The experiment is with linear polarizers in the viscoelastic phase.

The nematic phase made during experiments in the viscoelastic phase is concerved still after applying stress by closing the pistons back to the initial position. If a second experiment is performed in the same clay the pattern that evolves will follows the 'fractures' seen through the polarizers. This 'fractures' are observed both with linear and circular polarization. An example of this is shown in Figure 4.9 which show the last frame of an experiment with two different orientations of linear polarization and circular polarization.

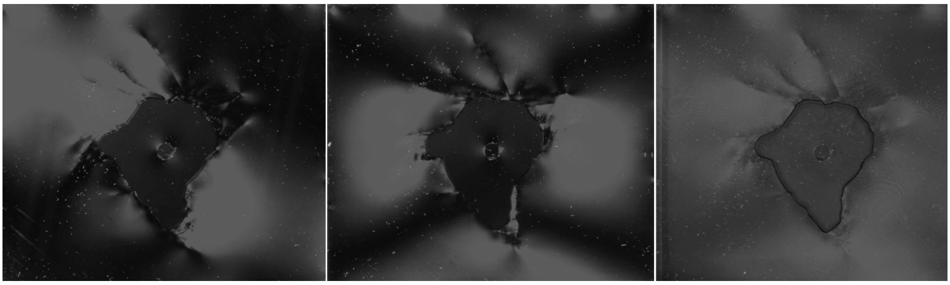

Figure 4.9: Experiment in Hele-Shaw cell with $C_s = 5 \cdot 10^{-3}$ and τ_w = 12:20 h. The first and second picture is with crossed linear polarizers, with the polarizers principal axis at 90° and 45° with respect to the direction of the piston movement. The third picture is shown with circular polarization.

The surface of the glass could have influence on the nematic phase observed. To get some knowledge of this effect an experiment in the viscoelastic phase is performed with no hole in the cell and the pistons move in the same direction, i. e. one piston pull and the other push the clay. The result of this experiment is shown in Figure 4.10. Here some birefringence is observed near both pistons but not in the bulk of the clay.

4.4 Experiment in Hele-Shaw cell with tracer particles

When using crossed polarizers the change in orientation of the clay particles are observed. To understand this further a few experiments are performed using silver nanoparticles to investigate flow in the bulk. The experiments with particles are done around the liquid/viscoelastic transition. Visual movement near the bubble are observed. Some analysis of this is described in section 4.6.2.

The particles dissolves easily in the clay solution and sediment in the initial liquid phase. An experiment with particles is shown in Figure 4.11. The patterns observed are similar to the patterns seen without particles.

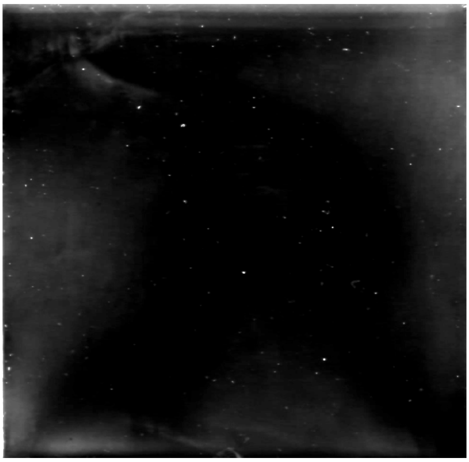

Figure 4.10: Experiment in Hele-Shaw cell with $C_s = 9.5 \cdot 10^{-3}$ and $\tau_w = 0{:}30$ h. The experiment is with linear polarizers in the viscoelastic phase and no hole in the cell. The pistons move in the same direction, i.e. one piston pull and the other push the clay suspension.

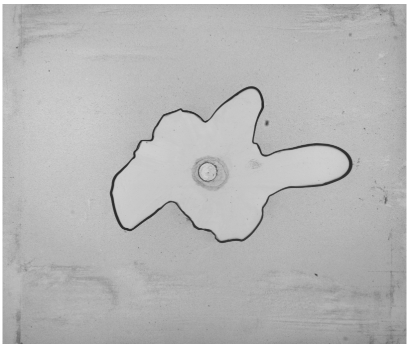

Figure 4.11: Experiment in Hele-Shaw cell with $C_s = 10^{-3}$ and $\tau_w = 16{:}10$ h, done with 0.7 g/L of silver nanoparticles.

4.5 Rheology experiments

Experiments in the rheometer is performed with 3 wt% laponite and distilled water. The different experiments have different waiting times before the measurements starts to check if the stress induced by the experiment have influence on the aging of the clay suspension. The experiments are shown in Figure 4.12 where the complex viscosity is plotted against time.

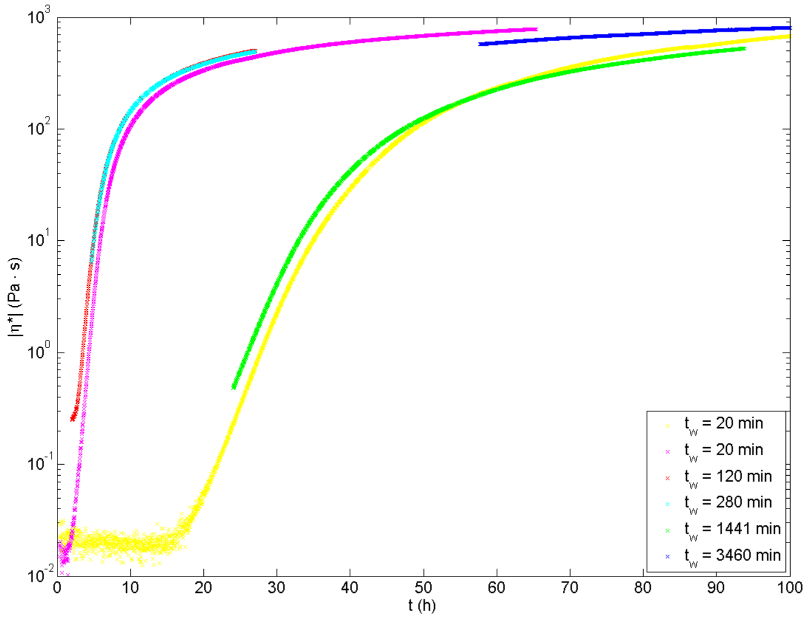

Figure 4.12: Results from the rheology experiments. Each experiment is with 3 wt% laponite dissolved in distilled water and with different waiting time before the measurement starts.

The experiments show no consistency and the complex viscosity show the sol-gel transition to be either at about 5 hours or 25 hours. With so big difference it is hard to transfer this to the Hele-Shaw cell. The time aspect in the cell is different from these results with a transition between liquid and viscoelastic at 33 hours.

4.6 Analysis

Analysis of the λ parameter and on experiments with tracer particles are shown in the following sections.

4.6.1 Analysis of λ

The parameter λ =width of finger/w is a important measure in liquid experiments. The time development of λ is found using the MATLAB code shown in appendix D . An example of this time development is shown in Figure 4.2. The results found for experiments in the liquid phase is shown in Figure 4.13.

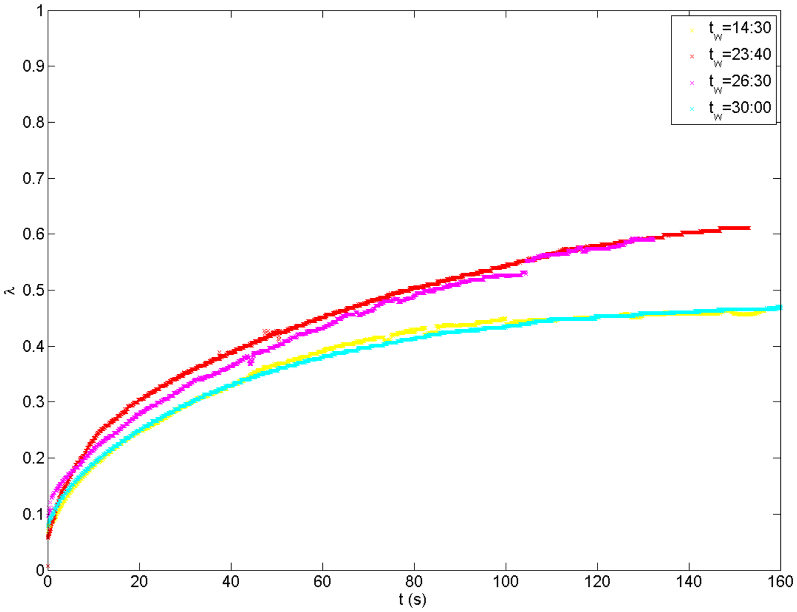

Figure 4.13: Analysis of λ in the liquid phase.

The λ parameter takes values between 0.47 and 0.61 in these experiments with different waiting times. It is no consistency between these experiments. The shortest and longest waiting time giving the smallest λ and the experiments with waiting times between these gives a higher value of λ.

4.6.2 Analysis of particle experiments

The experiment done with particles is analyzed using dynamic image correlation. A MATLAB script doing for is provided by PhD Baudouin Saintyves. This script check the concentration of particles in different arrays of one picture and compare this with another picture. The result could be seen as a vector-plot with the movement of the particles. This is shown in Figure 4.14.

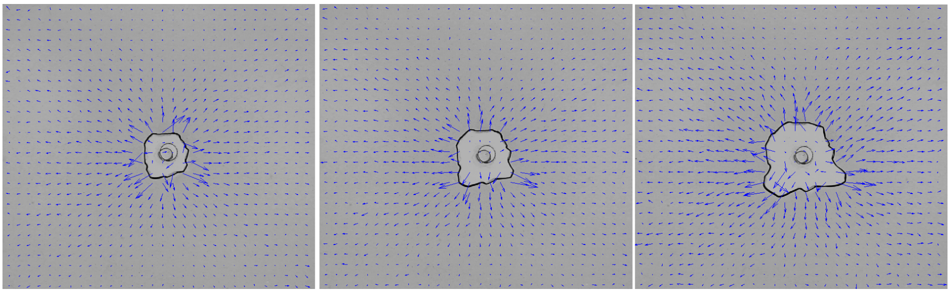

Figure 4.14: Experiment in Hele-Shaw cell with $C_s = 10^{-3}$ and τ_w = 16:30 h, done with 1.2 g/L of silver nanoparticles. Vector-plot from the dynamic image correlation indicating the movement in the bulk.

The direction of the movement is normal to the interface of the bubble with the largest movement in the direction of the pistons. This is the same as the expected stress field.

4.7 Discussion

In all experiments performed using crossed polarizers some birefringence are observed. If the nematic phase align the clay platelets parallel to the glass plate the change in polarization probably would not be seen. It is then obvious to think that the observed nematic phase contains clay platelets that stands normal to the glass surface. As the experiment is performed this could be due to that the clay flow over the glass surface. This configuration with standing clay platelets will give smallest friction between the suspension and the glass.

In the start of all experiments polarization is seen all around the initial bubble. In experiments performed with different linear polarizers we think that the clay platelets align with the stress field normal to the interface. The direction of the stress is also confirmed in the experiments done with tracer particles as the movement is in all direction out from the bubble. This is also in agreement with the experiment done by Shahin et. al. in 2011 [71]. These findings are general for all the experiments. In the continuation each of the observed phases are discussed.

4.7.1 Liquid phase

In the liquid phase two different patterns is observed, the X-shape and viscous fingers. The X-shape is related to the shear thinning behavior of laponite as described in section 4.2.2. The analysis of λ for the fingers show no consistency and this could be some complex fluid behavior related to the thixotropy. Different solutions will age in some way differently although the overall behavior is similar. It could be some heterogeneous parts in the cell or other uncertainties like the concentration of clay mineral. This will be discussed in a later section.

In the liquid phase it would occur a nematic phase between the finger and the piston as the finger come closer to the piston. This is a boundary effect and the nematic phase is formed when clay platelets are pulled together and align with the pistons. For the shear thinning phase this will affect the pattern and make the X-shape. It is also observed some nematic phase along the interface of the bubble. The nematic phase that occur in the liquid state is not stable. No bindings is obtained between the clay platelets.

The boundary conditions in the liquid phase is that the clay suspension have zero velocity at the boundary of the cell. For experiments done with particles, both experiment in the liquid phase and at the transition to viscoelastic phase is performed. In the liquid phase sedimentation in the cell is observed while at the transition this is not observed. Probably the particles sediment in the liquid phase for both but this is not observed for the viscoelastic phase because of the solid behavior of this. All the particles will already lay along the bottom glass plate. It could be an idea to use isodense particles if experiments like these should be performed in future studies.

Laponite follows Herschel-Bulkley fluid model according to the theory. This means that it shows shear thinning behavior with a yield stress. The shear thinning behavior is observed in the liquid state, but no quantitative analysis have been done to check this up to the model. It could be interesting for future studies to plot λ as a function of the velocity of the finger, u, and try to approximate the function of this through equation (2.36). As wetting of the glass surface is observed it would be expected that the effective surface tension needs to be considered. It would be interesting to see if the function of $\alpha(n)$, equation (2.38), proposed by Lindner et. al. in 2002 for a shear thinning Ostwald de Waele fluid (without yield stress) also is valid for the Herschel-Bulkley fluid model.

4.7.2 Viscoelastic phase

In the viscoelastic phase the sample will show both viscous and elastic behavior. For the liquid regime the boundary condition is as mentioned, that it is zero velocity at the side of the cell. For a solid this boundary velocity will be the same as the velocity of the pistons. That the observed pattern is round is a clear sign for viscous behavior.

How viscous or solid the clay is could be measured in a rheometer. The experiment performed in rheometer during this thesis show large inconsistency. The time scale in the rheology measurement is far from what observed in the cell. The longest measured sol-gel transition in the rheometer is 25 hours while the first experiment that shows elastic properties in the cell is for about 33 hours. The reasons for this are different measuring geometries. It could be worth trying a parallel-plate setup in the rheometer to get more similar geometries, but this will do it harder to seal it with oil to prevent evaporation. The sample volume will also be different.

The nematic phase that occur in the viscoelastic phase is similar to the one observed in the liquid phase. The clay platelets will align with the stress field out from the initial bubble. The difference is that patterns looking similar to fractures will occur in the nematic phase. These patterns are dark, both with circular and linear polarizers. This means that there is no nematic phase along these 'fractures'. The bubble often will propagate along these 'fractures' late in the experiment and also if the pistons are closed and reopened. An explanation of this could be that this is solid behavior and that the clay sample prepares actual fractures with aligning the clay platelets normal to the stress field. This could mean that the sample is heterogenous and these 'fractures' indicate the weakest places in the sample. A heterogenous sample means that the clay platelets have started to make clusters of different sizes which is expected for laponite.

In the viscoelastic regime the nematic phase that occur is stable and irreversible. When the sample is exposed for stress the clay platelets are aligned with the stress field and this change in orientation is a liquid behavior. The stability of the nematic phase on the other hand is an elastic property. The clay platelets is arrested in this state. It could be that the clay also makes clusters with the overlapping coin configuration as described by Jönsson et. al. in 2008 [70]. This is the configuration with the minimum energy and is expected to be stable.

4.7.3 Solid phase

In the solid phase simple plane cracks is expected with the direction normal to the pistons movement. In a few experiments this is observed, but in most the fractures leave in different directions and three cracks leaving the initial bubble are observed. The solid behavior with fractures is observed down to the concentration $5 \cdot 10^{-3}$ M of NaCl. This experiment is after about 600 hours. According to Ruzicka et. al. in 2011 [67] this arrested state is a gel formed by attractive forces. It is expected a shift in arrested state at NaCl concentration of $4 \cdot 10^{-3}$ M. Under this concentration the solid is expected to be a glass formed by repulsive forces. It could be interesting to find this transition with this Hele-Shaw setup. Then several experiment for smaller concentrations and longer waiting times need to be performed. It is expected that a repulsive glass will not give fractures.

The formation of a fracture could be dependent on the velocity. In this thesis different velocities are not considered. For higher speed the time of observation is shorter and will give a larger Deborah number and a more solid response. On the other side laponite is a shear thinning fluid with yield stress so experiments that is characterized as solid here could have a more viscous response for higher velocities. Experiments should be performed in the rheometer to get more knowledge go this behavior.

In some of the solid experiments the first sharp fracture tip widens for later times. Some birefringence 'fracture' patterns as described in the viscoelastic phase also occur. This could be due to bindings between clay platelets is broken and a more viscous response is seen. A more probable explanation is that the aging is different near the interface of the bubble than in the bulk of the sample. This is also observed by Shahin et. al. in 2011 [71]. Experiment observing this could be said to be solid near the interface and viscoelastic in the bulk which will be on the transition between these two phases. In experiments for longer waiting times it would be expected to see solid behavior in the whole sample and experiment on this should be done in future studies.

The viscoelastic/solid behavior described above could also be explained with that the sample is heterogenous. When finishing stirring the sample already have started to be a gel and according to Cummins in 2007 [61] the filtering will not break up clusters completely. In addition most of these experiments is for high NaCl concentration near the regime where phase separation is expected. It could be possible that there is large clusters of clay particles with viscous regimes inside on a small scale.

4.7.4 Uncertainties

As mentioned in the section above it is observed that the clay gelling under the preparation. This could give a heterogeneous initial state which could have influence on the aging of the clay suspension. For low concentration of NaCl the initial state will be a isotropic fluid. In the experiment done in the rheometer, distilled water is used and still a large deviation in results are observed. One explanation could be uncertainties in the clay concentration. The clay mineral is heated in an oven before inserted into a glove bag with N_2 environment. This is to prevent water to intercalate into the clay. It is reported by Ruzicka et. al. in 2004 [65] that laponite powder can contain up to 20 wt% of water. It is important that the dry powder is kept in an atmosphere without humidity. The humidity is not measured inside the glove bag so this could give a large uncertainty of the actual concentration of clay mineral. A change in concentration of clay mineral will have a large impact on the gelling time. This could be the explanation of the inconsistency of the λ parameter as well.

In this thesis the parameter NaCl concentration and waiting time have been considered. Other factors could have a large impact on the sample and needs to be investigated in future studies. The clay concentration has, as mentioned above, a large influence on the gelling time. Other parameters are the velocity of the pistons, aspect ratio of the cell, width of the cell, hight of the cell and the initial bubble in the cell. Changing these parameters could give even more information about the boundary conditions and the complex behavior of laponite.

Another factor that could have influence on the patterns and the formation of a nematic phase are roughness on the glass plates. It could be due to contamination or scratches at the surface. This is very hard to control but it needs to be considered as a source of error.

Chapter 5

Conclusion and future studies

5.1 Conclusion

In experiments performed during this thesis 3.0 wt% of laponite have been used and investigated with different concentrations of NaCl and different waiting times. Experiments have been performed in a Hele-Shaw cell and additional experiments in a rheometer. In the Hele-Shaw cell experiments have been done on the patterns in the cell and nematic phases have been investigated using different crossed polarizers. A few experiment were also performed using tracer particles.

A large range in time and concentration have been investigated and three different phases have been observed. The fluid phase, the viscoelastic phase and the solid phase. The experiments are summarized in the phase diagram shown in Figure 4.6. In the fluid phase the experiments are reversible and there is not found a stable change in the organization of clay particles. Both viscous fingers and shear thinning behavior is observed in this phase.

In the viscoelastic phase the sample shows both viscous and elastic properties. The viscous behavior is the overall round pattern and the formation of a nematic phase. Elastic properties is the roughness of the observed shape, the stability of the nematic phase and the observed 'fracture' patterns in the nematic phase. Such 'fracture' patterns are preparation for fractures to propagate there, with alignment of the clay platelets normal to the stress field.

In the solid phase almost no nematic phase is observed and the pattern consist sharp fractures penetrating the sample. The aging effect and the concentration of NaCl have a large impact on laponite as seen in the phase diagram. Different aging near the interface and in the bulk are observed. In addition large inconsistency is observed in the rheological measurement and in the analysis of the λ parameter. This could be due to uncertainties originating from the sample preparations and the concentration of laponite.

One conclusion to this thesis is that this is a new way to dynamically determine rheological properties related to the complex behavior of laponite and to better understand flow in complex fluids.

5.2 Future studies

In this thesis a large range in waiting time and NaCl concentration is considered. In future studies it could be interesting to perform experiments in a smaller range of these parameters and also to change other possible parameters such as the aspect ratio, hight of the cell and the velocity of the pistons. With many experiments with similar parameters a more precise analysis could be carried out. Especially experiments around the transitions between the phases fluid/viscoelastic and viscoelastic/solid are interesting.

In future studies the protocol of making clay sol/gels must be held strict to avoid humidity in the atmosphere containing the clay. It could be interesting to check if adjusting the pH will have any effect on the aging time. Experiments in a rheometer with parallel-plate setup should be performed because this is more similar the geometry in the Hele-Shaw cell than the coaxial cell geometry used here.

Analysis of λ as a function of the finger velocity could give information about the shear thinning behavior of laponite in the experiments with this behavior. It also could be interesting to analyze the finger/fracture velocity and changing different parameters in the experiment. If a more quantitative analysis is carried out it could be possible to check if it is in accordance with different rheological models, like the Herschel-Bulkley fluid model.

Another idea is to investigate different clay systems to see if similar effects are observed. Bentonite for example have a similar phase diagram as laponite, but have much larger diameter of the clay platelets [74]. Other swelling clay minerals could be interesting to investigate as well.

Appendix A

Notation used in this report

$\boldsymbol{B}$ or B	Magnetic field	T
$1/B$	$12\eta u w^2/\sigma b^2$	1
b	Width of gap in cell	m
C_s	Concentration of NaCl	M
C_w	Weight percent	%
c	Speed of light $= 3.00 \cdot 10^8$	m/s
c_R	Rayleigh wave speed	m/s
Ca	Capillary number $= \eta u/\sigma$	1
D_e	Deborah number	1
$\boldsymbol{E}$ or E	Electric field	N/C
E	Young's modulus	Pa
F_{ij}	Universal function	1
G	Shear modulus	Pa
G'	Storage modulus	Pa
G''	Loss modulus	Pa
$\mathcal{G}$	Mechanical energy released per unit area	$\mathrm{J/m^2}$
I	Electrolyte concentration	mol/L
$\boldsymbol{J}$	Volume current density	$\mathrm{A/m^2}$
K	Stress intensity factor	$\mathrm{N/m^{3/2}}$
k	Permeability	$\mathrm{m^2}$
k	Wavenumber	1/m
$\boldsymbol{n}$	Nematic director	1
n	Index of refraction	1
p	Pressure	Pa
r	Distance from the crack tip	m

S_2	Nematic order parameter	1
t	Time	s
t_w	Waiting time	s
T	Temperature	K
u	Finger-velocity	m/s
v	Fracture-velocity	m/s
w	Width of cell	m
x	Direction parallel to finger movement	m
y	Direction parallel to width of cell	m
Γ	Fracture energy	$\mathrm{J/m^2}$
$\boldsymbol{\gamma}$ or γ	Shear strain	1
$\dot{\boldsymbol{\gamma}}$ or $\dot{\gamma}$	Shear rate	1/s
ϵ	Width of gap/width of cell ratio $= b/w$	1
ϵ	Permittivity	$\mathrm{C^2/Nm^2}$
ϵ_0	Permittivity of free space $= 8.85 \cdot 10^{-12}$	$\mathrm{C^2/Nm^2}$
η	Viscosity	Pa·s
η^*	Complex viscosity	Pa·s
θ	Angel with respect to crack	rad
λ	Relativ width of finger, (finger width)$/w$	1
μ	Mobility	s/kg
μ	Permeability	$\mathrm{N/A^2}$
μ_0	Permeability of free space $= 4\pi \cdot 10^{-7}$	$\mathrm{N/A^2}$
ν	Poisson ratio	1
ρ	Density	$\mathrm{kg/m^3}$
ρ	Current density	$\mathrm{C/m^3}$
σ	Surface tension	N/m or Pa·m
$\boldsymbol{\sigma}$ or σ	Shear stress	Pa
σ_0	Threshold stress	Pa
τ_K	Retardation time $= \eta/G$	s
τ_M	Relaxation time	s
τ_w	Waiting time	s
ϕ	Velocity potential	$\mathrm{m^2/s}$
ω	Angular frequency	1/s

Appendix B

Motor settings

The motor used in this experiment is 'Translation Stage VT-80 2Phase-041' from PI miCos GmbH with the travel range 50 mm. The velocity range is from 0.001 mm/s to 20 mm/s and the maximum drag force is 50 N [75]. To control the motors the software Venus1Term is used and an overview of this is shown in Figure B.1.

To connect the motors press the menu 'Communication' and then 'Connect'. Axis 1 and 2 is each of the motors as shown in Figure B.1. That this is green shows that the motor is ok. The number over each axis show what position each motor have. To push the motors completely together the button at the left 'cal' is used. This will also set this position to zero. Where the zero position is could manually be set with the '« 0 »' button. To find the range of the motors the button 'rm' could be pressed. This will pull the motors maximum apart. To come back to the zero position the 'home' button can be pushed.

During experiments the velocity and the acceleration is set under 'Config' menu and then 'Dynamic-Parameters'. The motor is set to the zero position and how long the motors should be pulled apart is set in the number under axis 1 and 2. Then the button 'move abs' is used to move the motors to the absolute value indicated or the button 'move relative' is used to pull the piston relative from the start position.

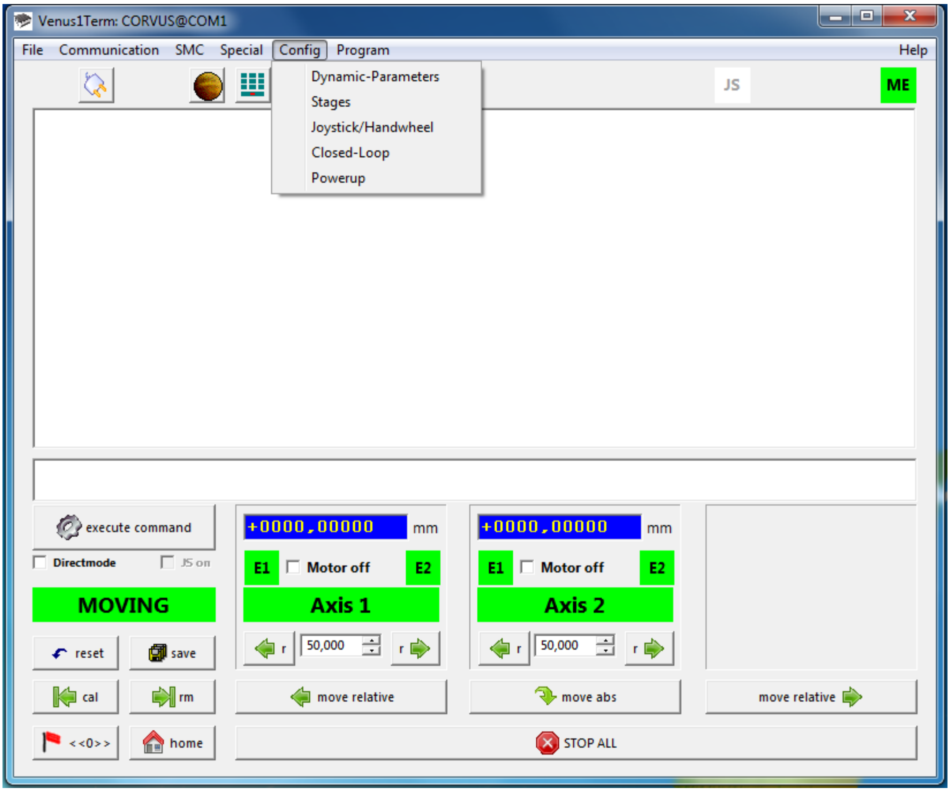

Figure B.1: An overview of the software Venus1Term used to control the motors.

Appendix C

Camera settings

C.1 Prosilica GX 1050

One camera used is a Prosilica GX 1050 from Allied Vision Technologies. According to the manufacturer, the resolution is 1024x1024, the max frame rate at full resolution is 112 fps and the exposure time could be between 10 μs and 60 s [76]. The program 'Measurements & Automation' is used to change the configuration. The camera is found under 'Devices and Interfaces', then 'NI-IMAQdx Devices' and then 'cam0: Allied Vision Technologies GX1050 (02-2400B)'. Then all the configurations could be set. In this thesis a frame rate of 30 fps is used. This could be set under 'Acquisition' and then 'AcquisitionFrameCount'. 'AquistionMode' is set to 'continuous' and this means that the camera needs to be stopped manually after started.

The exposure time is set under 'Exposure' and then 'ExposureTimeAbs'. The exposure time used in the experiments performed during this thesis is 1084 μs. Gain is set to 0 under 'Gain' and then 'GainRaw'. The gain needs to be matched with the exposure time. In general the gain should be as small as possible because the noise also will be gained. For short exposure time the light let into the camera is so little that it could be smart to use gain, but for longer exposure time the gain could be set to zero to prevent noise.

The resolution could be set under 'ImageFormat' and is set to the maximum value 1024 in both direction. An overview of the program is shown in Figure C.1. [1]

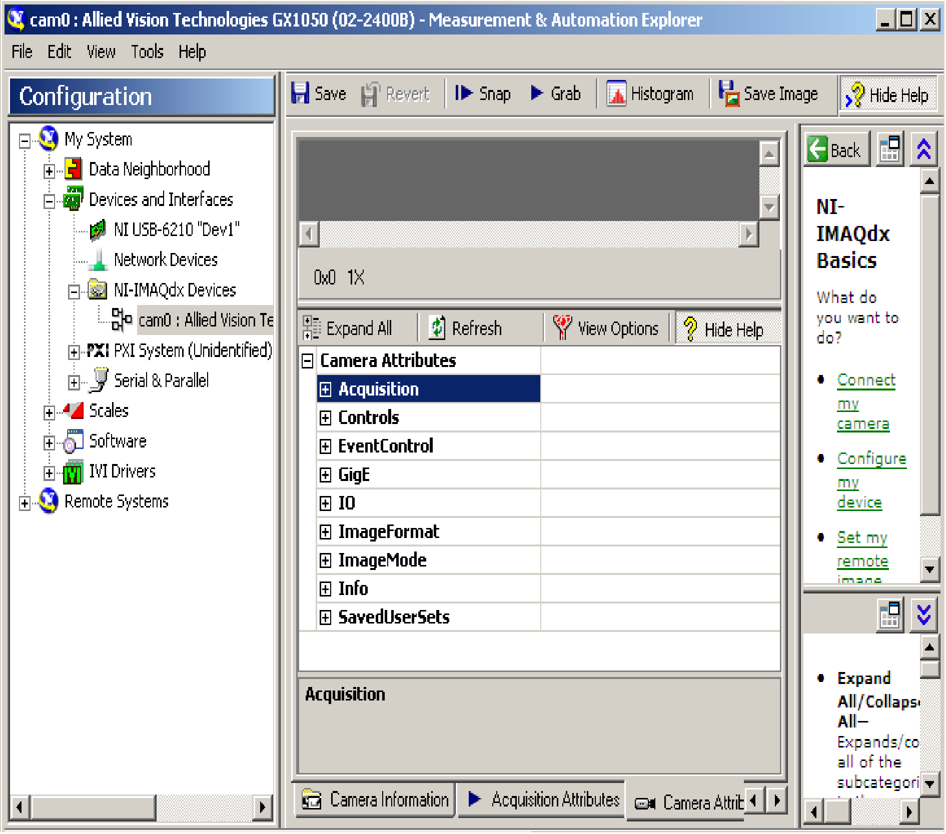

Figure C.1: Overview of the program 'Measurement & Automation' used to change the parameters on the camera. Figure adapted from [1].

The camera is controlled in the software labVIEW . Here the file 'GrabAvi.vi' is used. The block diagram from this file is shown in Figure C.2. In the program the camera name must be set to 'cam0' and then 'run' is pressed to start recording. Then the program will ask you to define the filename and where to put the file. When this is given the recording starts and run until 'stop' is pushed. Then the program saves the movie as an avi-file [1].

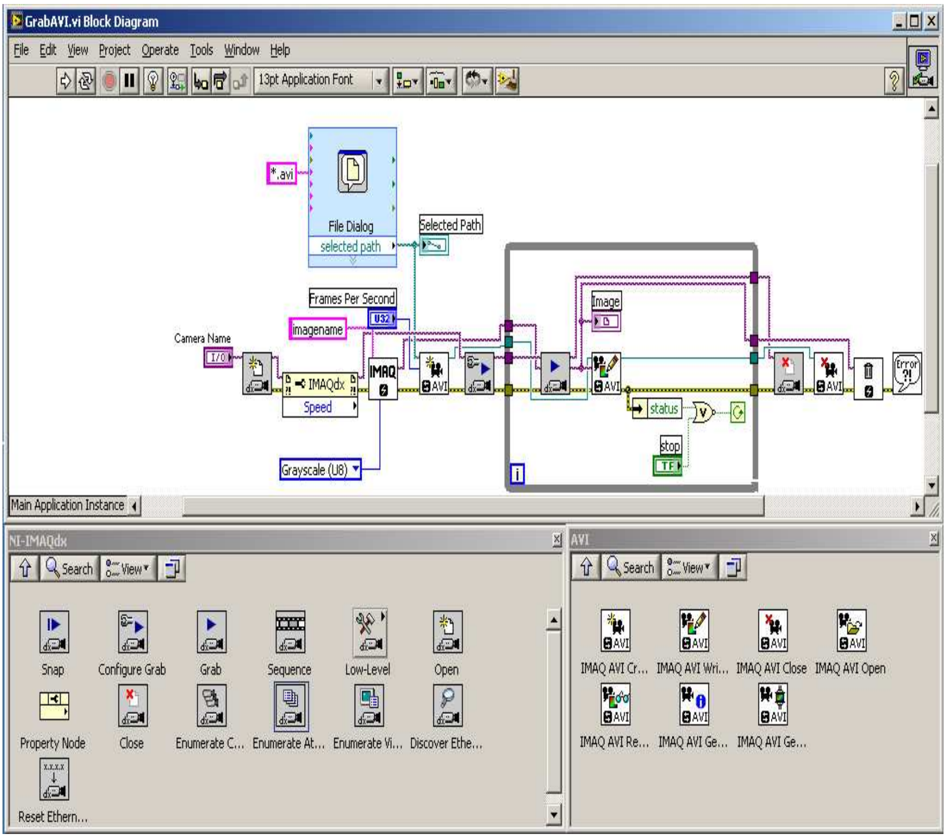

Figure C.2: Overview of the block diagram in labVIEW used to control the camera. Figure and program adapted from [1].

C.2 Canon EOS 600D

To see the birefringence better another camera is used to record the movies when using crossed polarizers. This is a Canon EOS 600D SLR camera with a resolution of 1920x1080 pixels and a frame rate of 25 fps using this resolution [77]. To control the camera from the PC the software following the camera, 'EOS Utility', is used.

After connecting the camera the software is started and 'Camera settings/Remote shooting' is chosen. Then 'Live view show' is pressed and the software window will look like Figure C.3. A live view of the camera appears. Then the manual zoom on the camera is set, and the auto focus is used to focus on the clay inside the cell. After that the camera is set to manually to remain the same setting under each recording. If the focus is not good this could be tuned in the software. To start recording the record button (with filled red circle) is pressed. The camera save the movie as an mov-file on the memory card. When the 'live view show' is closed the software ask you to download it to your computer.

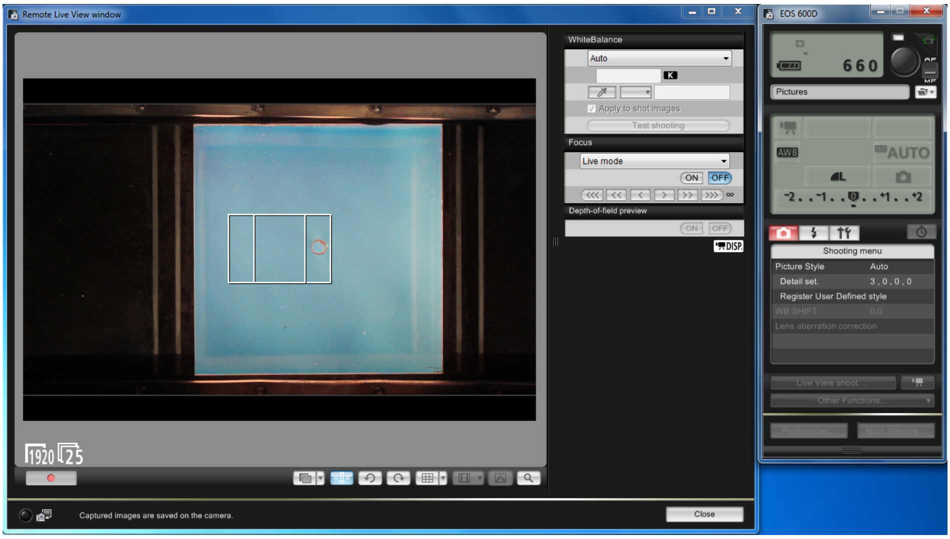

WhiteBalance Auto

Focus Live mode

Pictures

Shooting menu

Picture Style	Auto
Detail set.	3 , 0 , 0 , 0
Register User Defined style	
WB SHIFT	0,0
Lens aberration correction	

Captured images are saved on the camera.

Figure C.3: Overview of the EOS Utility software used to control the Canon EOS600D camera.

Appendix D

MATLAB code

D.1 Code for finding λ

For the liquid phase the λ parameter is an important measure. To find this the movies recorded of the experiment is analysed to find the time development of λ. Going through every frame of the movie is done using the code shown here.

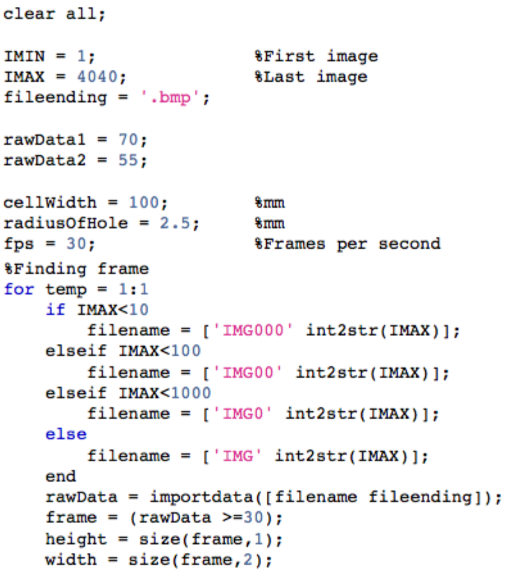

```
clear all;

IMIN = 1;                  %First image
IMAX = 4040;               %Last image
fileending = '.bmp';

rawData1 = 70;
rawData2 = 55;

cellWidth = 100;           %mm
radiusOfHole = 2.5;        %mm
fps = 30;                  %Frames per second
%Finding frame
for temp = 1:1
    if IMAX<10
        filename = ['IMG000' int2str(IMAX)];
    elseif IMAX<100
        filename = ['IMG00' int2str(IMAX)];
    elseif IMAX<1000
        filename = ['IMG0' int2str(IMAX)];
    else
        filename = ['IMG' int2str(IMAX)];
    end
    rawData = importdata([filename fileending]);
    frame = (rawData >=30);
    height = size(frame,1);
    width = size(frame,2);
```

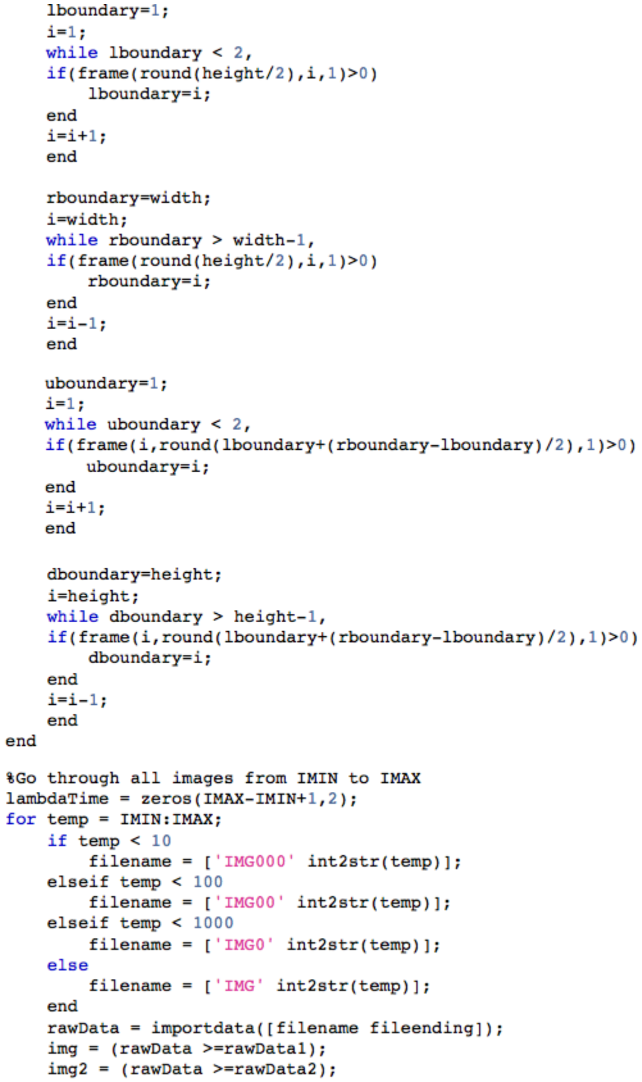

```
    lboundary=1;
    i=1;
    while lboundary < 2,
    if(frame(round(height/2),i,1)>0)
        lboundary=i;
    end
    i=i+1;
    end

    rboundary=width;
    i=width;
    while rboundary > width-1,
    if(frame(round(height/2),i,1)>0)
        rboundary=i;
    end
    i=i-1;
    end

    uboundary=1;
    i=1;
    while uboundary < 2,
    if(frame(i,round(lboundary+(rboundary-lboundary)/2),1)>0)
        uboundary=i;
    end
    i=i+1;
    end

    dboundary=height;
    i=height;
    while dboundary > height-1,
    if(frame(i,round(lboundary+(rboundary-lboundary)/2),1)>0)
        dboundary=i;
    end
    i=i-1;
    end
end

%Go through all images from IMIN to IMAX
lambdaTime = zeros(IMAX-IMIN+1,2);
for temp = IMIN:IMAX;
    if temp < 10
        filename = ['IMG000' int2str(temp)];
    elseif temp < 100
        filename = ['IMG00' int2str(temp)];
    elseif temp < 1000
        filename = ['IMG0' int2str(temp)];
    else
        filename = ['IMG' int2str(temp)];
    end
    rawData = importdata([filename fileending]);
    img = (rawData >=rawData1);
    img2 = (rawData >=rawData2);
```

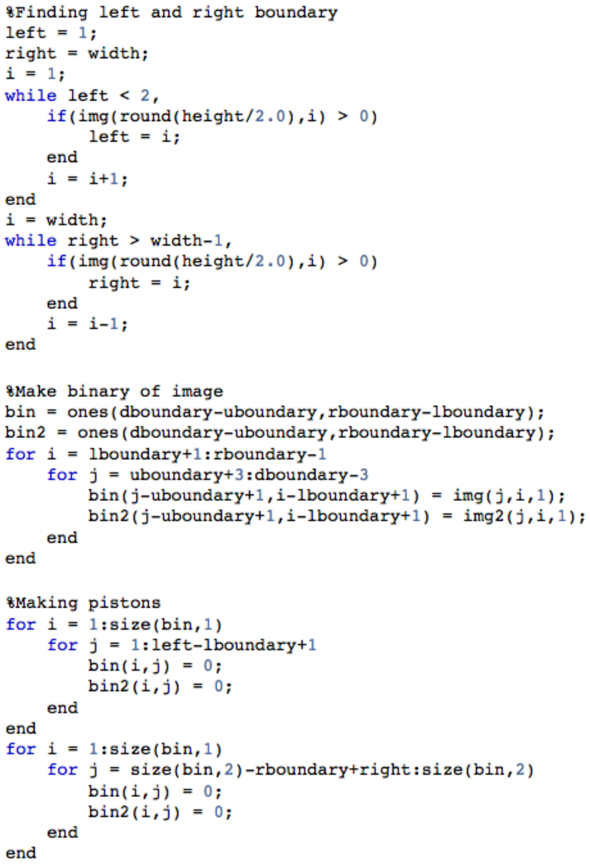

```
%Finding left and right boundary
left = 1;
right = width;
i = 1;
while left < 2,
    if(img(round(height/2.0),i) > 0)
        left = i;
    end
    i = i+1;
end
i = width;
while right > width-1,
    if(img(round(height/2.0),i) > 0)
        right = i;
    end
    i = i-1;
end

%Make binary of image
bin = ones(dboundary-uboundary,rboundary-lboundary);
bin2 = ones(dboundary-uboundary,rboundary-lboundary);
for i = lboundary+1:rboundary-1
    for j = uboundary+3:dboundary-3
        bin(j-uboundary+1,i-lboundary+1) = img(j,i,1);
        bin2(j-uboundary+1,i-lboundary+1) = img2(j,i,1);
    end
end

%Making pistons
for i = 1:size(bin,1)
    for j = 1:left-lboundary+1
        bin(i,j) = 0;
        bin2(i,j) = 0;
    end
end
for i = 1:size(bin,1)
    for j = size(bin,2)-rboundary+right:size(bin,2)
        bin(i,j) = 0;
        bin2(i,j) = 0;
    end
end
```

```
    %Finding bubblewidth
    radiusOfHolePxl = round(radiusOfHole*size(bin,1)/typecast(cellWidth,'double'))+1;
    u = 0;
    d = size(bin,1);
    i = 20;
    while u < 1,
        if(bin(i,round(size(bin,2)/2.0)) < 1)
            u = i;
        end
        i = i+1;
        if(i>size(bin,1))
            u = round(size(bin,1)/2.0)-radiusOfHolePxl;
            d = round(size(bin,1)/2.0)+radiusOfHolePxl;
            break
        end
    end
    i = size(bin,1)-round(3*u/8.0);
    while d > size(bin,1)-1,
        if(bin2(i,round(size(bin,2)/2.0)) < 1)
            d = i;
        end
        i = i-1;
        if(i<1)
            d = round(size(bin,1)/2.0)+radiusOfHolePxl;
            break
        end
    end


    %Calculate lambda
    lambdaTime(temp-IMIN+1,1) = (temp-1)/fps;
    lambdaTime(temp-IMIN+1,2) = (d-u)/typecast(size(bin,1),'double');      %bubbleWidth/cel
end

%Plot and save
dlmwrite('lambda.dat',lambdaTime,'\t')
figure
plot(lambdaTime(:,1),lambdaTime(:,2),'bx')
```

Appendix E

Poster from international workshop in Lofoten

At a international workshop on 'Soft matter physics and complex flows' in Lofoten May 22.-25. 2012 Phd Baudouin Saintyves presented some of the results found in this master thesis on a poster. The poster is seen on the next page.

FINGERING INSTABILITIES IN COMPLEX FLUIDS AND SOLIDS

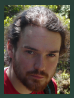

Baudouin Saintyves,
Olivier Dauchot, Elisabeth Bouchaud

@ SPHYNX

EXPERIMENTS

Classical Hele-Shaw cell

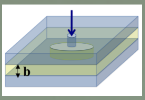

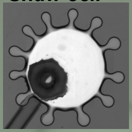

Control parameter :

b=0.5 ➡ 5mm

Sample radius: 80mm

Original design for displacement control

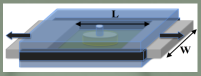

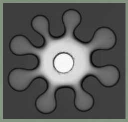

W=L=100mm b=2.1mm

Control parameter:

Vp=5mm/s

OBSERVATIONS AND RESULTS

IN A PURELY ELASTIC MATERIAL (POLYACRYLAMIDE)

An elastic instability?

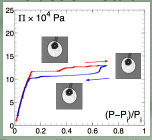

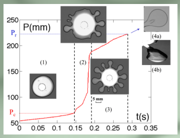

- Reversible ➡ elastic
- Hysteretic
- 4 stage phenomenon

Thickness profile determined by light absorption

Recession in the vicinity of the finger

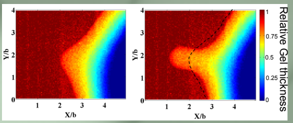

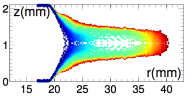

Growth of the finger with time

Shear modulus dependence?

- No dependence of the critical strain
- No significant dependence of the number of fingers

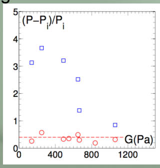

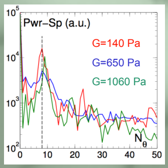

Confinement effect

- Non linear relation between width of finger l and gap size b
- Non linear relation between the inverse number of fingers and b

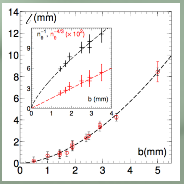

FROM LIQUID TO SOLID

In Maxwell Fluids

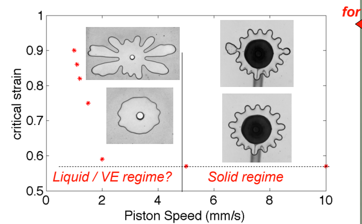

In collaboration with Serge Mora, LCVN, Université Montpelier 2

In laponite, from bubble to cracks

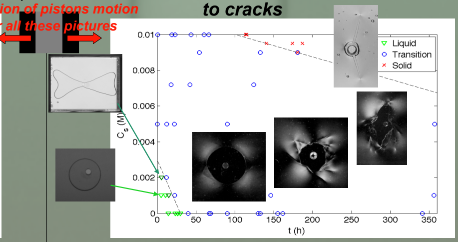

In collaboration with Kristian Hox and Jon Otto Fossum, NTNU

PERSPECTIVES

- Theoretical work and comparison with previous work on bending instabilities (see Mahadevan et al. (2012), Djondjorov et al.(2011))
- Pressure gradient dependence
- Characterisation of the VE regime in Maxwell fluids
- Image correlation analysis: particles in Laponite

Bibliography

[1] Cappelen, B. U. K. Experimental studies of finger and fracture instabilities in clays throughout the sol–gel transition. Master's thesis, NTNU, (2011).

[2] Ruzicka, B., Zulian, L., Zaccarelli, E., Angelini, R., Sztucki, M., Moussaïd, A., and Ruocco, G. Competing interactions in arrested states of colloidal clays. *Phys. Rev. Lett.* **104**, 085701 (2010).

[3] Ruzicka, B., Zaccarelli, E., Zulian, L., Angelini, R., Sztucki, M., Mossaïd, A., Narayanan, T., and Ruocco, G. Observation of empty liquids and equilibrium gels in a colloidal clay. *Nature Mater.* **10**, 56–60 (2011).

[4] Saffmann, P. G. and Taylor, G. The penetration of a fluid into a porous medium or Hele-Shaw cell containing a more viscous liquid. *Proc. Roy. Soc. A* **245**, 1242, 312–329 (1958).

[5] Barnes, H. A., Hutton, J. F., and Walters, K. *An Introduction to Rheology.* Elsevier, 2nd edition, (1989).

[6] Krishnan, J. M., Deshpande, A. P., and Kumar, P. B. S., editors. *Rheology of Complex Fluids.* Springer Science+Business Media, (2010).

[7] Schramm, G. *A Practical Approach to Rheology and Rheometry.* Haake Instruments Inc, 2nd edition, (2000).

[8] Reiner, M. The Deborah number. *Phys. Today* **17**, 1, 62 (1964).

[9] Morariu, S., Lămătic, I.-E., and Bercea, M. Rheological behavior of smectite aqueous dispersions. *Rev. Roum. Chem.* **54**, 975–980 (2009).

[10] Bonn, D., Kellay, H., Tanaka, H., Wegdam, G., and Meunier, J. Laponite: What is the difference between a gel and a glass. *Langmuir* **15**, 7534–7536 (1999).

[11] Ponton, A., Warlus, S., and Griesmart, P. Rheological study of the sol–gel transition in silica alkoxides. *J. Colloid Interf. Sci.* **249**, 209–216 (2002).

[12] Rao, M. A. *Rheology of fluid and semisolid foods.* Springer Science + Buisiness Media, 2nd edition, (2007).

[13] Gado, E. D., de Arcangelis, L., and Coniglio, A. Viscoelastic properties at the sol–gel transition. *Macromol. Symp.* **171**, 79–86 (2001).

[14] Kroon, M., Wegdam, G. H., and Sprik, R. Dynamic light scattering studies on the sol–gel transition of a suspension of anisotropic colloidal particles. *Phys. Rev. E* **54**, 6, 6541–6550 (1996).

[15] Martin, J. E. and Wilcoxon, J. P. Critical dynamics of the sol–gel transition. *Phys. Rev. Lett.* **61**, 3, 373–376 (1988).

[16] Martin, J. E., Adolf, D., and Wilcoxon, J. P. Viscoelasticity near the sol-gel transition. *Phys. Rev. A* **39**, 3, 1325–1332 (1989).

[17] Schapery, R. A. A theory of crack initiation and growth in viscoelastic media: I. theoretical development. *Int. J. Fracture* **11**, 1, 141–159 (1975).

[18] Dally, J. Dynamic photoelastic studies of fracture. *Exp. Mech.* **19**, 349–361 (1979).

[19] Schapery, R. A. A theory of crack initiation and growth in viscoelastic media: II. approximate methods of analysis. *Int. J. Fracture* **11**, 3, 369–388 (1975).

[20] Schapery, R. A. A theory of crack initiation and growth in viscoelastic media: III. analysis of continuous growth. *Int. J. Fracture* **11**, 4, 549–562 (1975).

[21] Bonamy, D. and Bouchaud, E. Failure of heterogeneous materials: A dynamic phase transition? *Phys. Rep* **498**, 1–44 (2011).

[22] Adda-Bedia, M. and Amar, M. B. Crack dynamics in elastic media. *Philos. Mag. B* **78**, 2, 97–102 (1998).

[23] Vasil'ev, A. From the Hele-Shaw experiment to integrable systems: A historical overview. *Compl. anal. oper. theory* **3**, 551–585 (2009).

[24] Pitts, E. Penetration of fluid into Hele-Shaw cell: The Saffman–Taylor experiment. *J. Fluid Mech.* **97**, 53–64 (1980).

[25] Lindner, A., Bonn, D., Poiré, E. C., Amar, M. B., and Meunier, J. Viscous fingering in non-Newtonian fluids. *J. Fluid Mech.* **469**, 237–256 (2002).

[26] McLean, J. W. and Saffman, P. G. The effect of surface tension of fingers in a Hele-Shaw cell. *J. Fluid Mech.* **102**, 455–469 (1981).

[27] Vanden-Broeck, J.-M. Fingers in a Hele-Shaw with surface tension. *Phys. Fluids* **26**, 6, 2033–2034 (1983).

[28] Park, C. W. and Homsy, G. M. The instability of long fingers in Hele-Shaw flows. *Phys. Fluids* **28**, 6, 1583–1585 (1985).

[29] Lindner, A., Bonn, D., and Meunier, J. Viscous fingering in complex fluids. *J. Phys: Condens Matter* **12**, A477–A482 (2000).

[30] Rabaud, M., Couder, Y., and Gerard, N. Dynamics and stability of anomalous Saffman–Taylor fingers. *Phys. Rev. A* **37**, 3, 935–947 (1988).

[31] Kessler, D. A. and Levine, H. Theory of the Saffman–Taylor "finger" pattern. *Phys. Rev. A* **33**, 4, 2621–2633 (1986).

[32] Tabeling, P., Zocchi, G., and Libchaber, A. An experimental study of the Saffman–Taylor instability. *J. Fluid Mech.* **177**, 67–82 (1987).

[33] Tanveer, S. Surprises in viscous fingering. *J. Fluid Mech.* **409**, 273–308 (2000).

[34] Bensimon, D., Kadanoff, L. P., Liang, S., Shraiman, B. I., and Tang, C. Viscous flows in two dimensions. *Rev. Mod. Phys.* **58**, 4, 977–1002 (1986).

[35] Park, C. W. and Homsy, G. M. Two-phase displacement in Hele-Shaw cells: theory. *J. Fluid Mech.* **139**, 291–308 (1984).

[36] Tabeling, P. and Libchaber, A. Film draining and the Saffman–Taylor problem. *Phys. Rev. A* **33**, 1, 794–796 (1986).

[37] Saffman, P. G. Viscous fingering in Hele-Shaw cells. *J. Fluid Mech.* **173**, 73–94 (1986).

[38] Ledesma-Aguilar, R., Pagonabarraga, I., and Hernández-Machado, A. Three-dimensional aspects of fluid flows in channels ii. effects of meniscus and thin film regimes on viscous fingers. *Phys. Fluids* **19**, 102113 (2007).

[39] Maxworthy, T. Experimental study of interface instability in a Hele-Shaw cell. *Phys. Rev. A* **39**, 11, 5863–5867 (1989).

[40] Mora, S. and Manna, M. Saffman–Taylor instability for generalized Newtonian fluids. *Phys. Rev. E* **80**, 016308 (2009).

[41] Hirata, T. Fracturing due to fluid intrusion into viscoelastic materials. *Phys. Rev. E* **57**, 2, 1772–1779 (1998).

[42] Lemaire, E., Levitz, P., Daccord, G., and Damme, H. V. From viscous fingering to viscoelastic fracturing in colloidal fluids. *Phys. Rev. Lett.* **67**, 15, 2009–2012 (1991).

[43] Miranda, J. A. and Widom, M. Radial fingering in Hele-Shaw cell: a weakly non linear analysis. *Physica D* **120**, 315–328 (1998).

[44] Bonn, D., Kellay, H., Bräunlich, M., Amar, M. B., and Meunier, J. Viscous fingers in complex fluids. *Physica A* **220**, 60–73 (1995).

[45] Lindner, A., Bonn, D., and Meunier, J. Viscous fingering in shear-thinning fluid. *Phys. Fluids* **12**, 2, 256–261 (2000).

[46] Fast, P., Kondic, L., Shelley, M. J., and Palffy-Muhoray, P. Pattern formation in non-Newtonian Hele-Shaw flow. *Phys. Fluids* **13**, 5, 1191–1212 (2001).

[47] Hecht, E. *Optics.* Addison Wesley, 4th edition, (2002).

[48] Griffiths, D. J. *Introduction to electrodynamics.* Pearson Education, 3rd edition, (2008).

[49] Hemmen, H., Ringdal, N. I., Azevedo, E. N. D., Engelsberg, M., Hansen, E. L., Méheust, Y., Fossum, J. O., and Knudsen, K. D. The isotropic–nematic interface in suspensions of Na-fluorohectorite synthetic clay. *Langmuir* **25**, 21, 12507–12515 (2009).

[50] Strobl, G. *Condensed Matter Physics.* Springer-Verlag Berlin Heidelberg, 1st edition, (2004).

[51] Chandrasekhar, S. *Liquid Crystals.* Cambridge University Press, 2nd edition, (1992).

[52] Hansen, E. L. Colloidal dispersions of clay nanoplatelets – optical birefringence and x-ray scattering studies of nematic phases. Master's thesis, NTNU, (2008).

[53] Bergaya, F., Theng, B. K. G., and Lagaly, G. *Handbook of Clay Science*. Elsevier Ltd., (2006).

[54] Rozynek, Z. J. *Experimental Studies of Self-organization from Electrically Polarized Clay Particles*. PhD thesis, NTNU, (2011).

[55] Fossum, J. O. Physical phenomena in clays. *Physica A.* **270**, 270–277 (1988).

[56] Fossum, J. O. Flow of clays. *Eur. Phys. J. Special Topics* **204**, 41–56 (2012).

[57] da Silva, G. J., Fossum, J. O., DiMasi, E., Måløy, K. J., and Lutnæs, S. B. Synchrotron x-ray scattering studies of water intercalation in a layered synthetic silicate. *Phys. Rev. E* **66**, 011303 (2002).

[58] Laponite: performance additives. `http://www.laponite.com/pdfs/laponite.pdf`, (2011). [Online; accessed 16-April-2012].

[59] Bonn, D., Tanaka, H., Wegdam, G., Kellay, H., and Meunier, J. Aging of a colloidal "Wigner" glass. *Europhys. Lett.* **45**, 1, 52–57 (1999).

[60] Bonn, D., Coussot, P., Huynh, H. T., Bertrand, F., and Debrégeas, G. Rheology of soft glassy materials. *Europhys. Lett.* **59**, 5, 786–792 (2002).

[61] Cummins, H. Z. Liquid, glass, gel: The phases of colloidal laponite. *J. Non-Crystal. Solids* **353**, 3891–3905 (2007).

[62] Mourchid, A., Delville, A., Lambard, J., Lécolier, E., and Levitz, P. Phase diagram of colloidal dispersions of anisotropic charged particles: Equilibrum properties, structure and rheology of laponite suspensions. *Langmuir* **11**, 1942–1950 (1995).

[63] Mourchid, A., Lécolier, E., Damme, H. V., and Levitz, P. On viscoelastic, birefringent and swelling properties of laponite clay suspensions: Revisited phase diagram. *Langmuir* **14**, 4718–4723 (1998).

[64] Tanaka, H., Meunier, J., and Bonn, D. Nonergodic states of charged colloidal suspensions: Repulsive and attractive glasses and gels. *Phys. Rev. E* **69**, 031404 (2004).

[65] Ruzicka, B., Zulian, L., and Ruocco, G. Routes to gelation in a clay suspension. *Phys. Rev. Lett.* **93**, 258301 (2004).

[66] Joshi, Y. M., Reddy, G. R. K., Kulkarni, A. L., Kumar, N., and Chhabra, R. P. Rheological behavior of aqueous suspensions of laponite: new insights into aging phenomena. *Proc. R. Soc. A* **464**, 469–489 (2008).

[67] Ruzicka, B. and Zaccarelli, E. A fresh look at the laponite phase diagram. *Soft Matter* **7**, 1268–1286 (2011).

[68] Ruzicka, B., Angelini, L. Z. R., Sztucki, M., Moussaïd, A., and Ruocco, G. Arrested state of clay–water suspendsions: Gel or glass? *Phys. Rev. E* **77**, 020402(R) (2008).

[69] Jabbari-Farouji, S., Tanaka, H., Wegdam, G. H., and Bonn, D. Multiple nonergodic disordered states in laponite suspensions: A phase diagram. *Phys. Rev. E* **78**, 061405 (2008).

[70] Jönsson, B., Labbez, C., and Cabane, B. Interaction of nanometric clay platelets. *Langmuir* **24**, 20, 11406–11413 (2008).

[71] Shahin, A., Joshi, Y. M., and Ramakrishna, S. A. Interface-induced anisotropy and the nematic glass/gel state in jammed aqueous laponite suspensions. *Langmuir* **27**, 14045–14052 (2011).

[72] Shaukat, A., Sharma, A., and Joshi, Y. M. Squeeze flow behavior of (soft glassy) thixotropic material. *J. Non-Newton. Fluid Mech.* **167–169**, 9–17 (2012).

[73] Morariu, S. and Bercea, M. Effect of temperature and aging time on the rheological behaviour of aqueous poly(ethylene glycol)/laponite RD dispersion. *J. Phys. Chem. B* **116**, 48–54 (2012).

[74] Abend, S. and Lagaly, G. Sol–gel transition of sodium montmorillonite dispersion. *Appl. Clay Sci.* **16**, 201–227 (2000).

[75] Translation Stags VT-80. `http://www.pimicos.com/web2/en/1,4,210,vt80.html`, (2011). [Online; accessed 16-April-2012].

[76] Allied Vision Technologies Canada Inc. *AVT Prosilica GX*, v2.0.0 edition, (2011).

[77] Canon inc. *CanonEOS600D Instruction Manual*, (2011).